Accepted Manuscript

Synthesis, Biological Characterization and Molecular Modeling Insights of Spirochromanes as Potent HDAC Inhibitors

Florian Thaler, Loris Moretti, Raffaella Amici, Agnese Abate, Andrea Colombo, Giacomo Carenzi, Maria Carmela Fulco, Roberto Boggio, Giulio Dondio, Stefania Gagliardi, Saverio Minucci, Luca Sartori, Mario Varasi, Ciro Mercurio

PII: S0223-5234(15)30347-0

DOI: 10.1016/j.ejmech.2015.11.010

Reference: EJMECH 8200

To appear in: *European Journal of Medicinal Chemistry*

Received Date: 4 August 2015

Revised Date: 7 October 2015

Accepted Date: 5 November 2015

Please cite this article as: F. Thaler, L. Moretti, R. Amici, A. Abate, A. Colombo, G. Carenzi, M.C. Fulco, R. Boggio, G. Dondio, S. Gagliardi, S. Minucci, L. Sartori, M. Varasi, C. Mercurio, Synthesis, Biological Characterization and Molecular Modeling Insights of Spirochromanes as Potent HDAC Inhibitors, *European Journal of Medicinal Chemistry* (2015), doi: 10.1016/j.ejmech.2015.11.010.

Graphical abstract

Synthesis, biological characterization and molecular modeling insights of spirochromanes as potent HDAC inhibitors

Florian Thaler*, Loris Moretti, Raffaella Amici, Agnese Abate, Andrea Colombo, Giacomo Carenzi, Maria Carmela Fulco, Roberto Boggio, Giulio Dondio, Stefania Gagliardi, Saverio Minucci, Luca Sartori, Mario Varasi, and Ciro Mercurio*

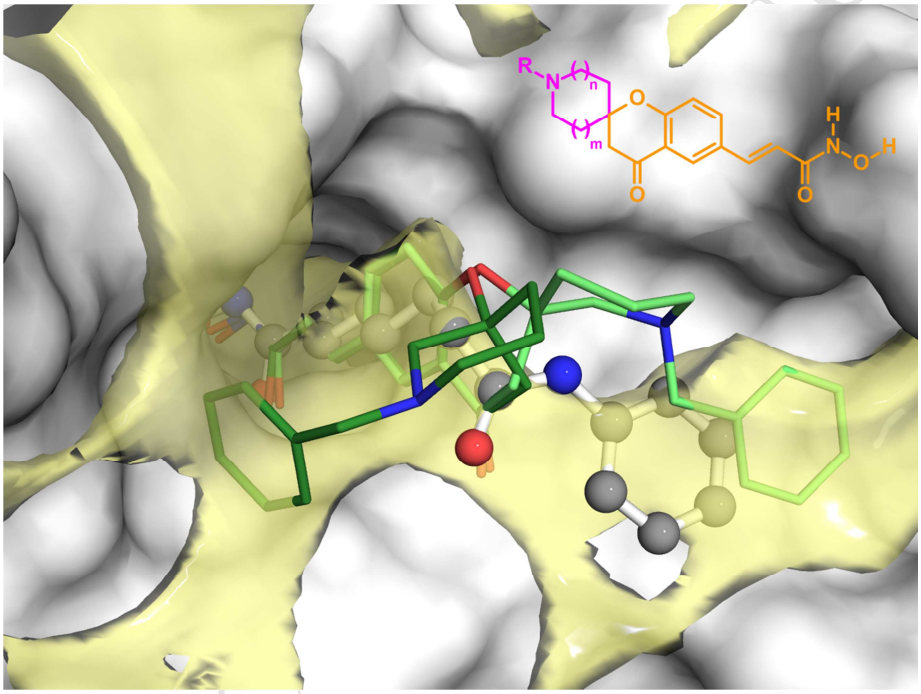

Synthesis, Biological Characterization and Molecular Modeling Insights of Spirochromanes as Potent HDAC Inhibitors

Florian Thaler,[a,b*] Loris Moretti,[b] Raffaella Amici,[a,b] Agnese Abate,[c,b,d] Andrea Colombo,[e,f] Giacomo Carenzi,[c,b,g] Maria Carmela Fulco,[c,b] Roberto Boggio,[a,h] Giulio Dondio,[e,i] Stefania Gagliardi,[e,j] Saverio Minucci,[k,l] Luca Sartori,[c,b] Mario Varasi,[c,b] and Ciro Mercurio[c*]

[a] Genextra Group, Congenia srl, Genextra Group, Via Adamello 16, 20139 Milan, Italy;

[b] Drug Discovery Program, Department of Experimental Oncology, European Institute of Oncology, Via Adamello 16, 20139 Milan, Italy;

[c] Genextra Group, DAC srl, Genextra Group, Via Adamello 16, 20139 Milan, Italy;

[d] current address: Sbarro Health Research Organization, Bio Life Science Building-Temple University, 1900 North 12th Street, Philadelphia, PA 19122-6099 (USA);

[e] NiKem Research srl, Via Zambeletti 25, 20021 Baranzate (MI), Italy;

[f] current address: Teva Pharmaceuticals Fine Chemicals, Strada Statale Briantea, 23892 Bulciago (Italy);

[g] current address: Fondazione Istituto Insubrico di Ricerca per la Vita, Via Lepetit, 34, 21040 Gerenzano (Italy);

[h] current address: NBE Bioanalytics, Merck Serono, Italy;

[i] current address: Aphad srl, Via della Resistenza 65, 20090 Buccinasco (MI), Italy;

[j] current address: Flamma S.p.A., Via Bedeschi 22, 24040 Chignolo d'Isola (BG), Italy;

[k] European Institute of Oncology, Via Adamello 16, 20139 Milan, Italy;

[l] University of Milan, University of Milan, Via Celoria 26, 20133 Milan, Italy

* Correspondance to F.Thaler, C. Mercurio European Institute of Oncology, Via Adamello 16, 20139 Milan (Italy), T +390294375130; F +390294375138; Email: florian.thaler@ieo.eu, ciro.mercurio@ieo.eu.

Abbreviations: HDAC, histone deacetylases; HAT, histone acetyltransferases; SQM, Semi-empirical Quantum Mechanics; CYP, cytochrome P450.

Abstract

In the last decades, inhibitors of histone deacetylases (HDAC) have become an important class of anti-cancer agents. In a previous study we described the synthesis of spiro[chromane-2,4'-piperidine]hydroxamic acid derivatives able to inhibit histone deacetylase enzymes. Herein, we present our exploration for new derivatives by replacing the piperidine moiety with various cycloamines. The goal was to obtain highly potent compounds with a good *in vitro* ADME profile. In addition, molecular modeling studies unravelled the binding mode of these inhibitors.

Keywords

Epigenetics, histone deacetylases, antiproliferation, privileged structures, molecular modeling

1. Introduction

Post-translational modifications on histones have been demonstrated to be essential regulators of the gene expression.[1] Among these, acetylation and deacetylation of the ε-amino groups of lysine residues represent crucial modifications of these proteins. The positively charged lysines present at the *N*-terminal tail of the histones allow tight binding of negatively charged DNA around them. This strong histone-DNA interaction blocks the binding sites of promoters and thus inhibits gene transcription. The neutralization of the charge through the acetylation of the amino groups of the lysines reduces the electrostatic interactions with the DNA leading to the nucleosome unwrapping.[2] This unfolding of the chromatin allows the transcriptional factors to access the gene promoter regions with the consequent gene expression. The balance between hyperacetylation and hypoacetylation is maintained by two counteracting enzyme families, namely histone acetyltransferases (HATs) and histone deacetylases (HDACs). Currently, 18 different human HDACs have been identified and are grouped into two families: the classical HDACs and the silent information regulator (Sir)-related proteins (sirtuins). Classical HDACs are Zn^{2+} dependent metalloenzymes and based on their sequence homology to the yeast analogues can be further divided into 4 classes. Class I comprises HDACs 1, 2, 3, and 8, class IIa HDACs 4, 5, 7, 9, class IIb HDACs 6 and 10 and class IV HDAC11.[3-9] Sirtuins, also known as class III HDACs, form a structurally and mechanistically distinct group and comprise Sirt1 to

Sirt7. Class III HDACs are characterized by their dependency on NAD^+ as cofactor.[10] Since the acetylation status of histones is critical for the gene expression modulation and cell fate, there is no surprise that its dysregulation is involved in the development of several cancers. Recent studies revealed that HDACs are responsible for the deacetylation of several non-histones too, such as proteins relevant for tumorigenesis, for cancer cell proliferation, and for immune functions.[11, 12]

In the past two decades the inhibition of HDACs has emerged as an attractive therapy to reverse aberrant epigenetic changes associated with cancer, inflammation and neurodegenerative diseases.[13-18] Several compounds reached clinical investigations and they demonstrated to be particularly efficacious in the treatment of different hematological malignancies.[19-21] So far, the clinical studies have culminated in the market approval of four distinct chemical entities (see Fig. 1). The hydroxamic acid vorinostat, known also as SAHA or Zolinza®[22], and the cyclic depsipeptide romidepsin, known FK228 or Istodax®,[23, 24] have been approved for the treatment of the cutaneous T–cell lymphoma (CTCL). The disulfide romidepsin, which is converted in cells into the active (reduced) form,[24, 25] has also been approved for the treatment of peripheral T-cell lymphoma (PTCL) as well as the hydroxamate belinostat, known also as PXD101 or Beleodaq®[26, 27]. Finally, on February 2015 the FDA approved oral panobinostat (known also as LBH589 or Farydak®) in combination with bortezomib and dexamethasone in patients with recurrent multiple myeloma.[28] Despite these successes, the known HDAC inhibitors are less efficacious in other tumors, in particular in solid malignancies. Therefore, there is still a need to develop HDAC inhibitors with a better clinical profile.[19, 20, 29]

(Insert Figure 1 here)

In previous studies we described a spiropiperidine hydroxamic acid scaffold with potent HDAC inhibitory activity.[30] Structure-activity relationship studies (SAR) showed that modifications on the spirochromane core moiety had a substantial influence on the biological activities. The shift of the *N*-hydroxyacrylamide moiety or the replacement of the chromane ring by

spirobenzofuran generally furnished less active compounds. Furthermore, the exploration at the 4-oxo moiety demonstrated that the ketone group is critical for the target inhibition. In fact, modification of this group was detrimental for HDAC and antiproliferative activity. On the other hand, various *N*-substitutions on the piperidine group were well tolerated, and no major differences in the activities between these compounds were found. Considering that HDAC inhibitors are composed by a Zn^{2+} binding moiety, a spacer, which can be further divided into linker and connecting unit, and a cap group,[31, 32] this minor effect of the different modifications could be ascribed to an outside orientation of the *N*-substituents as the cap group.[33] Based on these observations we further explored this scaffold in order to find more active inhibitors maintaining their good ADME properties. For this purpose, various cycloamines were studied as replacement of the piperidine moiety. In the present study, we describe the synthesis of spirochromane azetidines, pyrrolidines, azepanes and piperidin-3yl derivatives with various *N*-substitutents as well as their biological activity in detail. At the same time, molecular modeling investigations were performed on a number of spirochromane inhibitors. Hence, molecular docking combined with Semi-empirical Quantum Mechanics (SQM) optimization allowed us to elucidate the ligand-binding mode of these molecules and to understand their SAR at the atomic level.

2. Results and Discussion

The synthesis of compounds **1a** to **1c** has been previously described.[30, 33]

The secondary amines **15**–**18** were prepared starting from commercially available 2-hydroxy-5-bromoacetophenone (**2**) as illustrated in Scheme 1. Cyclization of compound **2** with *N*-BOC protected cycloamine-ones in methanol in presence of pyrrolidine gave the spirocycles **3–6**, which were then coupled with methylacrylate in presence of palladium acetate [$Pd(OAc)_2$], tri(2-methylphenyl)phosphine ($P(o\text{-}tol)_3$), triethylamine (TEA) affording the spirocyclic acrylic methyl esters **7–10**. The methyl esters **7** and **9** were hydrolyzed with sodium hydroxide (NaOH) in a water/dioxane mixture, while intermediates **8** and **10** were treated with hydrogen chloride (HCl) in acetic acid (AcOH). The resulting carboxylic acids were coupled with NH_2OTHP (*O*-(tetrahydropyran-2-yl)hydroxylamine) in presence of EDC (*N*-(3-dimethylaminopropyl)-*N*'-

ethylcarbodiimide hydrochloride) and HOBt (*N*-hydroxybenzotriazole). Cleavage of the THP protecting group with HCl in diethylether or dioxane gave the requisite hydroxamic acids **15–18**.

(Insert Scheme 1 here)

N-substituted spirocycles **31a–h** to **34a–h** were prepared starting from the spirocyclic acrylic methyl esters **7–10** by cleaving the *tert*-butyloxycarbonyl (BOC) protecting group with HCl in dioxane as outlined in Scheme 2. The free piperidines **19–22** were then either directly alkylated, acylated or reductively alkylated using sodium triacetoxyborohydride ($NaBH(OAc)_3$) as reducing agent. Hydrolysis of methyl esters **23a–h** to **26a–h** with NaOH in a water/dioxane mixture or HCl in acetic acid and subsequent introduction of the hydroxamic acid according to the procedure described above for compounds **15–18** (Scheme 1) furnished the requisite *N*-hydroxy-spirochromaneacrylamides **31-h** to **34a-h**.

(Insert Scheme 2 here)

The synthesis of the pure enantiomers of the *N*-benzyl-spiro(chromane-2,3'-pyrrolidine) analogues **32i** and **32j** was accomplished by attaching (S)-(6-methoxynaphthalen-2yl)propionic acid to the free amine **20**. The resulting two diastereoisomers were separated by normal phase column chromatography and subsequent re-crystallisation from *i*-PrOH (Scheme 3). Subsequently, the chiral auxiliary group was cleaved in HCl in acetic acid under microwave (MW) irradiation providing the corresponding amino acids **35** and **36**, which were then converted into the methyl esters **37** and **38**. The following steps to obtain the requisite enantiomeric hydroxamic acids **32i** and **32j** were carried out according to the procedures of the racemic **32d** as outlined in Scheme 2.

(Insert Scheme 3 here)

Scheme 4 summarizes the preparation of the [1'-benzyl-4-oxo-spiro(chromane-2,3'-piperidine)-6-yl]acrylhydroxamide enantiomers **33i** and **33j**. Spiropiperidine **5** was first deprotected in acidic conditions. The coupling with (R)-2-acetoxy-2-phenylacetic acid, separation of the two resulting diastereoisomers by column chromatography and removal of the chiral auxiliary were performed following the previously described method for the single enantiomer of 4-oxo-spiro(chromane-2,3'-piperidine).[34] The free piperidines of the separated enantiomers **39** and **40** were then protected with BOC anhydride. Heck reaction of the BOC protected compounds **41** and **42** with methyl acrylate in presence of $Pd(OAc)_2$, $P(o\text{-}tol)_3$ and TEA afforded the acrylic acid methyl esters, which were converted to the desired hydroxamic acids **33i** and **33j** following the procedures described for the racemic spiropiperidine **33d** as outlined in Scheme 2.

(Insert Scheme 4 here)

The putative HDAC inhibitors were profiled *in vitro* for their activity against the enzymes and the ability to block proliferation of tumor cells. The inhibitory effect of the compounds was assessed using a commercially available fluorescent based assay with partially purified HeLa nuclear extracts as enzyme source, which is according to the manufacturer's instruction a rich source of HDACs 1 and 2 (http://www.enzolifesciences.com/BML-AK500/fluor-de-lys-hdac-fluorometric-activity-assay-kit/). A comparative protein expression analysis of some HDACs between HeLA nuclear extract and total HeLa extract was performed in house and the Western blot results are in line with the manufacturer statements (see Fig. 2). Furthermore, reducing the protein expression of HDACs 1, 2 and 3 by sequential immunoprecipitation in the HeLa nuclear extract demonstrated that the observed histone deacetylase activity of HeLa nuclear extract is mainly imputable to HDAC1 and HDAC2 and not to HDAC3.

(Insert Figure 2 here)

The results are summarized in Table 1, which includes also the biological data of vorinostat as well as the 4-oxo-spiro(chromane-2,4'-piperidine) series **1a** to **1c** as references[30, 33]. The most

potent spiro(chromane-2,3'-azetidines) were the 1-methyl-indol-3-yl and the benzyl analogues **31f** and **31d** with IC_{50} values of 0.062 and 0.067 μM, respectively. On the other end, the acetyl derivative **31b** had with an IC_{50} value of 0.485 μM the lowest activity within this subseries. Major variations in activity were observed for the spiro(chromane-2,3'-pyrrolidine) and spiro(chromane-2,3'-piperidine) subseries. The 2-phenylethyl derivative **32g** exhibited an IC_{50} value of 0.027 μM, and its spiro(chromane-2,3'-piperidine) analogue **33g** was even more active inhibiting at 1 nM. The acetyl substituent emerged also in these two sub-series to be detrimental: compound **32b** (IC_{50} = 0.955 μM) was substantially less active than all other examples within the subseries of the spiropyrrolidines. Furthermore, the acetyl analogue **33b** had an IC_{50} value of 0.207 μM and was equipotent to the methyl (0.237 μM) and to the ethyloxycarbonyl (0.232 μM) inhibitors **33a** and **33c**. The 2-phenylethyl derivative **34g** was, with an IC_{50} value 0.056 μM, the most potent compound among the spiro(chromane-2,4'-azepane) analogues, and almost six times more active than the acetyl and the ethyloxycarbonyl analogues **34b** and **34c** (IC_{50} values of 0.323 and 0.300 μM, respectively). In summary, several compounds within all four cycloamine subseries emerged to be potent HDAC inhibitors, some of them were more potent than their corresponding spiro(chromane-2,4'-piperidine) analogues.[30, 33]

(Insert Table 1 here)

Furthermore, we evaluated the biochemical selectivity profile of some selected inhibitors considering HDAC2 and HDAC3 as representatives of HDACs of class I and HDAC6 as representative of class II HDACs. As shown in Table 3, the potency of the tested spirochromanes as well as for vorinostat was in the in the nanomolar range. Neither vorinostat nor any of the spiro derivatives showed preferential activity versus any of the isoforms, and thus the studied inhibitors can be classified as typical pan HDAC inhibitors.

(Insert Table 2 here)

The antiproliferative activities of the HDAC inhibitors were determined against three tumor cell lines of different tissue origin: K562 (chronic myelogenous leukaemia cell line), A549 (carcinomic human alveolar basal epithelial cells) and HCT116 (human colon cancer cells). As shown in Table 1, several compounds had a significantly higher antiproliferative activity than their spiro-2,4'-piperidine analogues. In specific, the indolyl derivative **31f** was the most potent compound in K562 cell line among the spiro(chromane-2,3'-azetidines) with an IC_{50} value of 0.046 μM, and showed together with the benzyl analogue **31d** a superior cellular activity in the A549 and HCT116 cell line than the other spiro(chromane-2,3'-azetidines). On the contrary, the acetyl spirocycle **31b** resulted substantially less potent than the other examples in the antiproliferative assays with IC_{50} values more than 10 μM in all three cell lines. The indolyl derivatives **32f** and **34f** were the most potent compounds also within the spiro(chromane-2,3'-pyrrolidine) and spiro(chromane-2,4'-azepane) series in the K562 cell line. Furthermore, these two compounds, the benzyl and the 2-phenylethyl analogues **32d**, **34d**, **32g** and **34g** as well as the methyl and para fluorobenzyl spiroazepanes **34a** and **34e** exhibited IC_{50} values lower than 100 nM in HCT116 cells. The methyl analogue **33a** emerged as the most active compound within the spiro(chromane-2,3'-piperidine) subseries in the K562 and A549 cell lines with IC_{50} values of 0.056 and 0.103 μM, respectively. Compound **33a**, the 2-phenylethyl **33g** and the indolyl analogues **33f** had a superior antiproliferative activity in HCT116 cells than the other spirochromane-2,3'-piperidines. Furthermore, we found that the unsubstituted spiropiperidine **17** was substantially more potent than the other free amines **15**, **16**, and **18**. In specific, compound **17** exhibited antiproliferative activity in the three cell lines with IC_{50} values of 0.555 μM (K562), 0.714 μM (A549) and 0.228 μM (HCT116), respectively. Overall, the antiproliferative activity of the spirocyclic inhibitors was generally higher in K562 and HCT116 cells than in the A549 cell line. In particular, thirteen compounds exhibited cellular growth inhibition with IC_{50} values ranging between 0.040 and 0.100 μM in HCT116 cells and resulted to be substantially more potent than vorinostat (IC_{50}=0.757 μM) and the previously disclosed spiropiperidine reference compounds **1a-c** (IC_{50} values of 0.477 μM, 0.777 μM and 0.201 μM, respectively). All four cycloamine subclasses are present in this list and we find indolyl, (4-fluoro)benzyl, 2-phenylethyl and methyl analogues for the various *N*-substitutions. On the other hand, unsubstituted and acyl spirocycles, in particular the acetyl derivatives, exhibited in general a lower cellular potency in all three cell lines.

With exception of the achiral spiro(chromane-2,3'-azetidine) and spiro(chromane-2,4'-piperidine) subseries, the other compounds discussed above were prepared and biologically tested as racemic mixtures. Thus, in order to gain insights if there are differences in the biological activities of stereoisomers, the pure enantiomers of the benzyl substituted spiro(chromane-2,3'-pyrrolidine) **32d** (**32i** and **32j**, respectively) and spiro(chromane-2,3'-piperidine) hydroxamic acid derivatives **33d** (**33i** and **33j**, respectively) were prepared and tested. The (–)-spiropyrrolidine **32i** exhibited an IC_{50} value of 26 nM in the enzymatic assay, which is virtually identical to that of the (+)-enantiomer (37 nM). Both enantiomers were equipotent as cell growth inhibitors in the three tested cell lines. Nonetheless compound **32i** was around 5 times more active than **32a** in the enzyme inhibitory assay, the two compounds exhibited comparable antiproliferative activity in K562 and A549 cells. It is often difficult to rationalize a link between the biochemical activity and the cellular potency on the sole basis of the pharmacodynamic properties of a molecule. In fact, several factors contribute to the activity in cells, such as cellular membrane permeability, sub-cellular compartmentalization, and cellular mechanisms for efficiently extruding xenobiotica. All these contributions could justify an observed discrepancy between biochemical and cellular potency.

A similar behavior was found for the two enantiomerically pure spiro(chromane-2,3'-piperidine) derivatives **33i** and **33j**. Also in this case, no significant differences in their biochemical inhibitory activity with IC_{50} values of around 100 nM were observed between the two stereoisomers. In addition, both compounds had practically the same antiproliferative potency in the K562, A549 and HCT116 cell lines.

To elucidate the mode of interaction of spirochromanes inhibitors with class I HDAC enzymes molecular modeling studies were performed. The binding conformations were predicted with molecular docking and later optimized at the Semi-empirical Quantum Mechanics level as described in the Experimental section. For this study, the structure of HDAC1 in complex with an acetate molecule[35] and the structure of HDAC2 in complex with the inhibitor vorinostat[36] were prepared and used. These two structures were chosen to account for the conformation variability of the L2 loop, which is involved in the binding of the substrate and of the inhibitors as shown for HDAC8.[37] The ligand-binding determination procedure was applied first on three reference inhibitors: vorinostat, trichostatin A and panobinostat and the results (data not shown)

were in good agreement with the experiments (X-ray, binding affinities, etc.). Then, for the exploration of the binding mode of spirochromanes, several representative molecules were docked against the two protein structures. In particular, the *N*-methyl and the *N*-benzyl derivatives of all studied spiro-ring sizes (4, 5, 6, and 7 membered rings) were fitted into the binding sites and optimized. The well-accepted pharmacophoric model of Zn-binding HDAC inhibitors identifies four parts of the ligand based on its interactions with the target.[32] The 'zinc binding group' (ZBG) that in the case of vorinostat and the spirochromanes is the hydroxamic acid, the 'linker' making hydrophobic contacts along the channel (connecting the binding site to the outside), the 'cap' which is the part interacting with the outer surface of the enzyme and the 'connecting unit' between the linker and the cap, corresponding to the amide in vorinostat. In the case of the herein described inhibitors, the resulting binding mode with the HDAC proteins, in line with the pharmacophore, is presented in Fig. 3 and 4. In Fig. 3 the interaction of the common substructure of the spirochromanes is depicted and as expected the metal is coordinated through the hydroxamate group.

(Insert Figure 3 here)

In addition, this group, as described by Vanommeslaeghe et al.,[38] makes three polar interactions with residues histidine 140 and 141, and tyrosine 303. The next portion of the ligand structure, the propenyl-benzene, is the linker that extends toward the outside and fits into the channel making hydrophobic contacts with the glycine 149 and leucine 271. But the main feature of this interaction is the π–π stacking in between the conserved phenylalanine residues 150 and 205 as investigated by Zhou et al..[39] The connecting unit of the studied inhibitors is represented by the second ring of the chromane, specifically its carbonyl group is found in the same region as the amide’s one in vorinostat (see Fig. 4).

(Insert Figure 4 here)

In general, this part of the pharmacophore is characterized by an sp2 group.[32] It appears to serve more as a geometric constraint, to direct properly the cap group, instead of interacting with the target. This observation would explain the loss of activity observed by the replacement of this carbonyl with various non-sp2 atoms in ligands of the same chemotype previously published.[30] Some of these modifications were also submitted to the docking protocol and showed a lower SQM energy after optimization (data not shown). Lastly, the variable part of this series of ligands is found outside of the protein, as seen in Fig. 4, and it is the cap group of the pharmacophore interacting with the outer surface of the protein. To understand the role of the cap group in the HDAC ligand-protein complexes, the hydrophobic favorable interaction areas were visualized as shown in Fig. 4 (see the Experimental section for details). These regions, close to the protein surface, specify the areas where favorable interactions can be made with aliphatic atoms of the ligand. In the case of the studied inhibitors, the ring of variable size (4 to 7 atoms) attached to the chromanone moiety does not make any additional interaction while its *N*-derivative can to a certain extend. About these substitutions, a trend of the enzymatic values is observed for the various spirochromane series, in specific acetyl > methyl > benzyl > phenylethyl with the best activity for the phenylethyl and the worst for the acetyl (see Table 1). The explanation is likely to be related to the inhibitor's portion approaching the favorable hydrophobic interaction regions. When the acetyl is present, a sub-optimal binding with the target would be achieved because of the polarity of the group. While growing the size of the hydrophobic *N*-substituent from methyl to phenylethylene the inhibitor structure can fill a larger area enhancing the binding with the target. Furthermore, the hydrophobic interaction area extends in various directions around the opening of the channel (see Fig. 4), explaining the same level of activity for the different stereoisomers observed for the spiro(chromane-2,3'-pirrolidine) and spiro(chromane-2,3'-piperidine) (**32i**, **32j**, **33i** and **33j** in Table 1) and for different conformations of the symmetric ligands as resulting from docking solutions.

As already outlined our efforts were directed towards compounds with an excellent potency and retaining the ADME profile compared to vorinostat and the spiropiperidine references **1a**, **1b** and **1c**. Thus, we selected the hydroxamic acid derivatives, which demonstrated to be highly active in the biochemical assay and having IC_{50} values of $\leq$ 100 nM in at least one cell line for ADME studies. The chosen compounds were first tested for their metabolic oxidative Phase I stability in mouse and human. For this purpose the inhibitors were incubated in mouse and human hepatic

microsomal preparations at 37 °C and the percentage of non-metabolized product was assessed after 30 min.[33, 40, 41] As shown in Table 3, the most evident result is that all indolyl analogues were found to be highly metabolically instable in applied conditions, with the only exception of the azetidine derivative **31f** in human microsomes. In specific, more than 70% of compounds **32f**, **33f**, and **34f** were metabolized after 30 min of incubation. The benzyl derivative **31d** with 44% unmetabolized product after 30 min incubation in mouse and human hepatic microsomes resulted to be more stable than the pyrrolidine analogues **32d**, **32i**, and **32j** (more than 70% of the product was metabolized in mouse and human microsomes), and the azepane derivative **34d** (25% remaining in mouse and 19% in human microsomes). The methyl analogues **33a** and **34a** emerged as the most stable compounds with a comparable or in some cases even superior stability than that of the spiropiperidine reference compounds **1a**, **1b**, and **1c**. For further in vitro characterizations, we decided not to investigate those compounds, which were metabolized over 80% in the microsome preparations at the given experimental conditions and thus resulted to be less stable than the lead spiropiperidine compounds. The additionally characterized inhibitors **31d**, **31f**, **32d**, **32g**, **33a**, **34a** and **34g** exhibited a good solubility, being in particular ≥ 500 μM at a pH value of 4.5. Furthermore, the same inhibitors did not exhibit any relevant inhibition of human cytochrome CYP1A2: the enzyme activity was blocked less than 10% at 10 μM concentration. More interaction was found for the other three tested human isoenzymes CYP 2C19, CYP 2D6 and CYP 3A4. In particular, the indolyl derivative **31f** blocked 84% of the CYP 3A4 enzyme activity at 10 μM concentration and the phenylethylene analogue **34g** 81% of the CYP 2C19 enzyme activity. On the other hand, the methyl derivative **34a** showed virtually no interference with the CYP 3A4 (12% inhibition at 10 μM), and the other two cytochromes (CYP 2C19 and CYP 2D6 activities less than 10% at at 10 μM). Eventually, the methyl derivatives **33a** and **34a**, the benzyl derivative **31d** and the phenethylene **32g** exhibited human cytochrome inhibitory activities comparable to the lead spiropiperidines and these results provided us a pool of compounds with a superior activity and with good in vitro ADME properties.

(Insert Table 3 here)

3. Conclusions

In previous studies we had identified a HDAC inhibitory scaffold based on privileged spiropiperidine structures.[30] Chemical modifications of the spirochromane moiety resulted in a number of compounds with good HDAC inhibitory potency as well as in vitro and in vivo ADME properties.[33, 42] Herein, we describe our further exploration of the scaffold through the replacement of the piperidine moiety by various cycloamines. The main goal was to achieve derivatives with good in vitro potency while maintaining their good ADME properties. For this purpose, we prepared and evaluated the biological activity of a series of spirochromane azetidines, pyrrolidines, azepanes and piperidin-3yl derivatives with various *N*-substitutents. Enzyme inhibition experiments revealed that the variation of the ring size ranging from 4 to 7 atoms attached to the chromanone moiety does not result in major changes in the biochemical activity. These observations are in agreement with molecular modeling studies, which showed that these moieties do not make any specific interaction with the protein, while the *N*-substitutent does interact to a various extend. In specific, the type of the group found at this position can contribute, positively or negatively, to the binding based on its complementarity with the identified favorable hydrophobic interaction regions at the outer surface of the enzyme. We found several potent inhibitors and selected 12 compounds, which exhibited a potent antiproliferative activity in tumor cell lines with IC_{50} values of less than 100 nM, for further in vitro ADME characterization. Hepatic microsomal stability and inhibition studies of selected human CYP450 isoenzymes allowed the identification of several candidates for further development. In specific, the methyl derivatives **33a** and **34a**, the benzyl derivative **31d** and the phenylethylen **32g** exhibited stability to Phase I oxidative conditions and cytochrome inhibitory activities comparable to the lead spiropiperidines.

4. Experimental

4.1 Chemistry. All reagents and solvents were of commercially available reagent grade quality and were used without further purification. Flash chromatography purifications were performed on Merck silica gel 60 (0.04–0.063 mm). Nuclear magnetic resonance spectra (^{1}H NMR and ^{13}C NMR) were recorded on a Bruker spectrometer at 300 MHz and 75 MHz, respectively, with TMS as internal standard, and, unless stated otherwise, at 300 K. The spectra are referenced in

ppm (δ) and coupling constants (*J*) are expressed in hertz (Hz). Standard abbreviations indicating multiplicity were used as follows: s=singlet, d=doublet, t=triplet, q=quartet, m=multiplet and bs=broad signal. HPLC purity of the target compounds was assessed either using a Waters 2777 Sample Manager and a Waters 1525 Binary HPLC Pump, equipped with a Waters 2996 diode array and a Micromass ZQ 2000 Single quadrupole (Waters) (**Method 1**, **2**, and **5**) or on an Acquity UPLC apparatus, equipped with a diode array and a Micromass ZQ single quadruple (Waters) (all other methods). The flow rate was adjusted to 2.0 mL/min for **Method 1** and **Method 5**, 0.3 mL/min for **Method 2**, and 0.6 mL/min for the other methods. Mobile phase A was composed by a mixture of water and acetonitrile (95:5) containing 0.1% TFA and mobile phase B by a mixture of water and acetonitrile (5:95) containing 0.1% TFA (**Methods 1**, **3**, and **7**). **Methods 2** and **5** were run with a mobile phase A composed by water containing 0.1% TFA and a mobile phase B composed by acetonitrile containing 0.1% TFA. Mobile phase A was composed by a mixture of water and methanol (95:5) containing 0.1% formic acid for **Method 4** and by water and acetonitrile (95:5) containing 0.07% formic acid for **Method 6**. Mobile phase B was composed by a mixture of water and methanol (5:95) containing 0.1% formic acid for **Method 4** and by water and acetonitrile (5:95) containing 0.05% formic acid for **Method 6**. Purity refers to UV detection at 254 nm.

METHOD 1: XBridge C8 (3.5 μm, 4.6 × 50 mm) column; gradient: 0.00-1.00 min (A: 95%, B: 5%), 1.00–8.00 min (A: 0%, B: 100%), 8.00–8.10 min (A: 90%, B: 10%), 8.10–8.50 min (A: 95%, B: 5%), 8.50–9.50 min (A: 95%, B: 5%).

METHOD 2: Atlantis dC18 (3 μm, 2.1 × 50 mm) column; gradient: 0.00–0.20 min (A: 95%, B: 5%), 0.20–5.00 min (A: 0%, B: 100%), 5.00–6.00 min (A: 0%, B: 100%), 6.00–6.10 min (A: 95%, B: 5%); 6.10–7.00 min (A: 95%, B: 5%).

METHOD 3: BEH C18 (1.7 μm, 2.1 × 50 mm) column; gradient: 0.00–0.25 min (A: 95%, B: 5%), 0.25–3.30 min (A: 0%, B: 100%), 3.30–4.00 min (A: 0%, B: 100%), 4.00–4.10 min (A: 95%, B: 5%); 4.10–5.00 min (A: 95%, B: 5%).

METHOD 4: BEH C18 (1.7 μm, 2.1 × 50 mm) column; gradient: 0.00–0.25 min (A: 95%, B: 5%), 0.25–3.30 min (A: 0%, B: 100%), 3.30–4.00 min (A: 0%, B: 100%), 4.00–4.10 min (A: 95%, B: 5%); 4.10–5.00 min (A: 95%, B: 5%).

METHOD 5: XBridge C8 (3.5 μm, 4.6 × 50 mm) column; gradient: 0.00-1.00 min (A: 95%, B: 5%), 1.00–7.50 min (A: 0%, B: 100%), 7.50–8.50 min (A: 0%, B: 100%), 8.10–8.50 min (A: 95%, B: 5%), 8.50–9.50 min (A: 95%, B: 5%).

METHOD 6: BEH C18 (1.7 μm, 2.1 × 50 mm) column; gradient: 0.00 (A: 98%, B: 2%), 0.00–3.00 min (A: 0%, B: 100%), 3.00–3.50 min (A: 0%, B: 100%), 3.50–4.50 min (A: 98%, B: 2%).

METHOD 7: BEH C18 (1.7 μm, 2.1 × 50 mm) column; gradient: 0.00–0.25 min (A: 95%, B: 5%), 0.25–3.30 min (A: 0%, B: 100%), 3.30–4.00 min (A: 0%, B: 100%), 4.00–4.10 min (A: 95%, B: 5%); 4.10–5.00 min (A: 95%, B: 5%).

(±)-6-bromo-4-oxo-spiro(chromane-2,3'-pyrrolidine)-1'-carboxylic acid *tert*-butyl ester (4)

A mixture of 2-hydroxy-5-bromoacetophenone (**2**, 5.00 g, 23.3 mmol), *N*-BOC pyrrolidin-3-one (4.30 g, 23.3 mmol) and pyrrolidine (3.87 mL, 46.5 mmol) in MeOH (20 mL) was heated under microwave irradiation for 4 h at 70 °C. The solution was concentrated and the crude mixture was purified by column chromatography (eluent: petroleum ether/EtOAc 95:5 to 7:3) to give the *tert*-butyl ester **4** (6.00 g, 68%) as a yellow solid. ^{1}H NMR ($CDCl_3$) δ (ppm): 8.00 (d, J = 2.64 Hz, 1H), 7.58 (dd, J = 8.80, 2.05 Hz, 1H), 6.89 (d, J = 8.80 Hz, 1H), 3.68–3.85 (m, 1H), 3.50–3.66 (m, 2H), 3.23–3.46 (m, 1H), 2.88–3.04 (m, 1H), 2.84 (d, J = 16.73 Hz, 1H), 2.23–2.39 (m, 1H), 1.84–2.02 (m, 1H), 1.47 (s, 9H). LC-MS: (ES+) MH^+-56: 326.

The bromospirochromanes **3**, **5** and **6** were prepared analogously starting from compound **2** and the appropriate amine following the procedure for intermediate **4** (see SI).

(±)-(E)-3-[1'-*tert*-Butoxycarbonyl-4-oxo-spiro(chromane-2,3'-pyrrolidine)-6-yl]-acrylic acid methyl ester (8)

A mixture of compound **4** (4.70 g, 12.3 mmol), $Pd(OAc)_2$ (55.1 mg, 0.246 mmol), $P(o\text{-}tol)_3$ (149 mg, 0.490 mmol), TEA (5.13 mL, 36.8 mmol), methyl acrylate (3.32 mL, 36.9 mmol) in dry

DMF (10 mL) was heated under N_2 atmosphere to 100 °C for 3 h. After cooling down to RT, the solution was poured into water (100 mL) and extracted with EtOAc (3 times 100 mL). The organic phase was dried over Na_2SO_4, filtered, and evaporated. The crude residue was recrystallized in petroleum ether:diisopropylether (1:1) to give the acrylic acid methyl ester **8** (3.85 g, 81%) as a light yellow solid. ^{1}H NMR ($CDCl_3$) δ (ppm): 8.06 (d, *J* = 2.05 Hz, 1H), 7.69 (dd, *J* = 8.80, 2.05 Hz, 1H), 7.66 (d, *J* = 15.85 Hz, 1H), 7.03 (d, *J* = 8.80 Hz, 1H), 6.41 (d, *J* = 16.14 Hz, 1H), 3.82 (s, 3H), 3.69–4.00 (m, 1H), 3.53–3.69 (m, 2H), 3.26–3.48 (m, 1H), 2.81–3.07 (m, 2H), 2.25–2.35 (m, 1H),1.81–2.05 (m, 1H), 1.48 (bs, 9H). LC-MS: (ES+) MH^+-56: 332.

The acrylic acid methyl esters **7**, **9** and **10** were prepared analogously starting from the corresponding bromo derivatives following the procedure for intermediate **8** (see SI).

(E)-3-[1'-*tert*-Butoxycarbonyl-4-oxo-spiro(chromane-2,3'-azetidine)-6-yl]-acrylic acid (11)

1 M NaOH (1.60 ml) was added to a solution of methyl ester **7** (450 mg, 1.20 mmol) in water (11 ml) and dioxane (22 ml). The mixture was stirred at RT overnight, then aqueous HCl 10% was added until reaching pH 7. The dioxane was removed and the residue was diluted with water. The aqueous layer was acidified to pH 5 with 10% aqueous HCl and the product was extracted with CH_2Cl_2. The collected organic phases were dried over Na_2SO_4 and concentrated to give the acrylic acid (430 mg, 100%) as a yellow solid. ^{1}H NMR (DMSO–d_6) δ (ppm): 2.33 (bs, 1H), 8.00 (dd, *J* = 8.51, 2.05 Hz, 1H), 7.96 (d, *J* = 2.35 Hz, 1H), 7.60 (d, *J* = 16.14 Hz, 1H), 7.20 (d, *J* = 8.51 Hz, 1H), 6.48 (d, *J* = 16.14 Hz, 1H), 4.01 (d, *J* = 9.68 Hz, 2H), 3.91 (d, *J* = 9.39 Hz, 2H), 3.20 (s, 2H), 1.39 (s, 9H); LC–MS: (ES+) MH^+–56: 304.

(±)-(E)-3-[1'-*tert*-Butoxycarbonyl-4-oxo-spiro(chromane-2,3'-pyrrolidine)-6-yl]acrylic acid (12)

5 mL of an 20% aqueous HCl (5 mL, 30 mmol) was added to a suspension of **8** (464 mg, 1.2 mmol) in glacial AcOH (5 mL). The mixture was stirred at 85 °C for 3 h and was then evaporated to give (±)-(E)-3-[4-oxo-spiro(chromane-2,3'-pyrrolidine)-6-yl]acrylic acid (370 mg, quantitative) as a white solid (hydrochloride salt). ^{1}H NMR (DMSO-d_6) δ (ppm): 12.30 (bs, 1 H), 9.79 (bs, 1 H), 9.67 (bs, 1 H), 7.87-8.19 (m, 2 H), 7.61 (d, *J*=15.85 Hz, 1 H), 7.08 (d, *J*=9.39 Hz,

1 H), 6.48 (d, *J*=15.85 Hz, 1 H), 3.24-3.66 (m, 4 H), 3.21 (d, *J*=17.02 Hz, 1 H), 3.11 (d, *J*=17.02 Hz, 1 H), 2.22-2.43 (m, 1 H), 2.10 (dt, *J*=13.86, 9.94 Hz, 1 H). LC-MS: (ES+) MH^+: 274.

TEA (0.50 mL, 3.6 mmol) was added to the suspension of (±)-(E)-3-[4-oxo-spiro(chromane-2,3'-pyrrolidine)-6-yl]acrylic acid (370 mg, 1.20 mmol) in 10 mL of CH_2Cl_2. After complete dissolution of the acid, BOC anhydride (314 mg, 1.44 mmol) was added and the mixture was stirred at RT for 1 h. The solution was poured into water (10 mL), neutralized with aqueous 5% citric acid solution and extracted with CH_2Cl_2. The organic phase was dried over Na_2SO_4, evaporated resulting in a white solid (406 mg, 91%) of acrylic acid **12**, which was used in the next step without purification. ^{1}H NMR (DMSO–d_6) δ (ppm): 7.78–8.20 (m, 2H), 7.57 (d, *J* = 15.85 Hz, 1H), 7.11 (d, *J* = 9.10 Hz, 1H), 6.46 (d, *J* = 15.85 Hz, 1H), 3.61 (d, *J* = 12.32 Hz, 1H), 3.25–3.55 (m, 3H), 3.15 (d, *J* = 16.73 Hz, 1H), 2.98 (d, *J* = 17.02 Hz, 1H), 2.11–2.28 (m, 1H), 1.88–2.11 (m, 1H), 1.27–1.52 (m, 9H); LC–MS: (ES+) MH^+–56: 318.

(±)-(E)-3-[1'-*tert*-Butoxycarbonyl-4-oxo-spiro(chromane-2,3'-piperidine)-6-yl]acrylic acid (13)

The methyl ester **9** (500 mg, 1.25 mmol) was suspended in 20 mL of a dioxane/water mixture (1:1). 1.62 mL 1 M NaOH was added and the solution was stirred at RT overnight. After acidification with an aqueous solution containing 5% citric acid the product was collected by filtration and dried giving the acrylic acid **13** (490 mg, quantitative) as a white solid. ^{1}H NMR (DMSO–d_6) δ (ppm): 12.30 (bs, 1H), 7.80–8.05 (m, 2H), 7.59 (d, *J* = 15.85 Hz, 1H), 6.83–7.11 (m, 1H), 6.44 (d, *J* = 16.14 Hz, 1H), 3.69–4.02 (m, 2H), 3.02–3.16 (m, 1H), 2.68–3.00 (m, 3H), 1.92–2.15 (m, 1H), 1.58–1.90 (m, 2H), 0.90–1.59 (m, 10H); LC–MS: (ES+) MH^+: 388.

The acrylic acid **14** was prepared following the procedure for intermediate **12** (see SI).

(E)-3-[4-Oxo-spiro(chromane-2,3'-azetidine)-6-yl]-*N*-hydroxy-acrylamide (15)

Acrylic acid **11** (430 mg, 1.20 mmol) was converted into the (E)-3-[1'-*tert*-butoxycarbonyl-4-oxo-spiro(chromane-2,3'-azetidine)-6-yl]-*N*-(tetrahydro-pyran-2-yloxy)-acrylamide (0.40 g, 73%, pale yellow solid) following the procedures for compound **16**. ^{1}H NMR (DMSO–d_6) δ (ppm): 11.13 (bs, 1 H), 7.93 (d, J=2.35 Hz, 1 H), 7.84 (d, J=8.80 Hz, 1 H), 7.50 (d, J=15.85 Hz, 1

H), 7.21 (d, J=8.51 Hz, 1 H), 6.50 (d, J=15.85 Hz, 1 H), 4.91 (bs, 1 H), 4.00 (d, J=9.39 Hz, 2 H), 3.93-3.98 (m, 1 H), 3.90 (d, J=9.39 Hz, 2 H), 3.44-3.74 (m, 1 H), 3.20 (s, 2 H), 1.48-1.84 (m, 6 H), 1.39 (s, 9 H); LC–MS: (ES+) MH^+–83: 375. Cleavage of the THP-protecting group (360 mg, 0.78 mmol) in CH_2Cl_2 (14 mL) was carried out by adding dropwise 1.90 mL 4 M HCl in dioxane and stirring the solution overnight at RT. The formed precipitate was filtered off, washed with CH_2Cl_2, dried to give the requisite hydroxamic acid **15** (154 mg, 65%, hydrochloride salt) as a white solid. ^{1}H NMR (DMSO–d_6) δ (ppm): 10.71 (bs, 1H), 9.42 (bs, 1H), 9.24 (bs, 1H), 7.92 (d, *J* = 2.05 Hz, 1H), 7.86 (dd, *J* = 8.80, 2.05 Hz, 1H), 7.46 (d, *J* = 15.85 Hz, 1H), 7.21 (d, *J* = 8.80 Hz, 1H), 6.46 (d, *J* = 15.55 Hz, 1H), 4.03 *J* = 4.33 (m, 4H), 3.31 (s, 2H); LC–MS: Method 1, rt=1.27; (ES+) MH^+: 275.

(±)-(E)-3-[4-Oxo-spiro(chromane-2,3'-pyrrolidine)-6-yl]-*N*-hydroxy-acrylamide (16)

TEA (0.271 mL, 1.95 mmol) was added to solution of the acrylic acid **12** (484 mg, 1.29 mmol) in CH_2Cl_2 (10 mL). The mixture was cooled down to 0 °C, and EDC (372 mg, 1.95 mmol) and HOBt (263 mg, 1.95 mmol) were added. The mixture was stirred at 0 °C for 3 h, then NH_2OTHP (182 mg, 1.56 mmol) was added and the mixture was stirred at RT overnight. The solution was washed with aqueous 5% $NaHCO_3$ solution and brine. The organic layer was then dried over Na_2SO_4 and evaporated. The crude residue was purified by column chromatography (eluent: CH_2Cl_2/MeOH 98:2) to give the *N*-(tetrahydro-pyran-2-yloxy)-acrylamide intermediate (499 mg, 89%) as a light yellow solid. ^{1}H NMR (DMSO-d_6) δ (ppm): 11.13 (bs, 1 H), 7.94 (d, *J*=2.05 Hz, 1 H), 7.81 (d, *J*=9.10 Hz, 1 H), 7.49 (d, *J*=15.55 Hz, 1 H), 7.12 (d, *J*=8.80 Hz, 1 H), 6.48 (d, *J*=16.43 Hz, 1 H), 4.91 (bs, 1 H), 3.81-4.03 (m, 1 H), 3.52-3.69 (m, 2 H), 3.32-3.52 (m, 3 H), 3.15 (d, *J*=17.02 Hz, 1 H), 2.98 (d, *J*=17.31 Hz, 1 H), 2.09-2.24 (m, 1 H), 1.90-2.09 (m, 1 H), 1.70 (bs, 3 H), 1.54 (bs, 3 H), 1.40 (m, 9 H). LC–MS: (ES+) MH^+: 473.

1 M HCl in Et_2O (5 mL, 5 mmol) was added dropwise to a solution of *N*-(tetrahydro-pyran-2-yloxy)-acrylamide intermediate (280 mg, 0.59 mmol) in CH_2Cl_2 (2 mL). The mixture was stirred at RT for 1 h. The precipitate was filtered off, washed with CH_2Cl_2, dried and collected giving the requisite hydroxamate **16** (108 mg, 57%) as a white solid (hydrochloride salt). ^{1}H NMR (DMSO–d_6) δ (ppm): 9.74 (bs, 1H), 9.61 (bs, 1H), 7.93 (d, *J* = 2.05 Hz, 1H), 7.82 (dd, *J* = 8.80, 2.05 Hz, 1H), 7.45 (d, *J* = 15.55 Hz, 1H), 7.09 (d, *J* = 8.80 Hz, 1H), 6.46 (d, *J* = 15.55 Hz, 1H),

3.55 (dd, *J* = 12.47, 5.72 Hz, 1H), 3.42 (bs, 2H), 3.24–3.37 (m, 1H), 3.20 (d, *J* = 17.02 Hz, 1H), 3.10 (d, *J* = 17.02 Hz, 1H), 2.21–2.43 (m, 1H), 2.09 (dt, *J* = 14.09, 9.83 Hz, 1H). LC–MS: Method 7, rt=0.91; (ES+) MH^+: 289.

The *N*-hydroxy-acrylamides **17** and **18** were prepared following the procedure for compound **16** (see SI).

(±)-(E)-3-[4-Oxo-spiro(chromane-2,3'-pyrrolidine)-6-yl]-acrylic acid methyl ester (20)

4 M HCl in dioxane (10 mL, 80 mmol) was added to a solution of spirocycle **8** (4.30 g, 11.2 mmol) in 15 mL CH_2Cl_2 and the mixture was stirred at RT for 1 h. The precipitate was filtered off, washed with CH_2Cl_2, dried and collected (3.3 g, 92%) giving the methyl ester **20** as a white solid (hydrochloride salt). ^{1}H NMR (DMSO–d_6) δ (ppm): 9.65 (bs, 2H), 7.97–8.11 (m, 2H), 7.70 (d, *J* = 15.85 Hz, 1H), 7.09 (d, *J* = 9.39 Hz, 1H), 6.60 (d, *J* = 16.14 Hz, 1H), 3.73 (s, 3H), 3.50–3.67 (m, 1H), 3.35–3.49 (m, 2H), 3.25–3.31 (m, 1H), 3.21 (d, *J* = 17.02 Hz, 1H), 3.11 (d, *J* = 17.02 Hz, 1H), 2.20–2.43 (m, 1H), 2.10 (dt, *J* = 14.01, 9.87 Hz, 1H). LC–MS: (ES+) MH^+: 288.

The acrylic acid methyl esters **19**, **21** and **22** were prepared following the procedure for intermediate **20** (see SI).

(±)-(E)-3-[1'-Benzyl-4-oxo-spiro(chromane-2,3'-pyrrolidine)-6-yl]-acrylic acid methyl ester (24d)

A suspension of spirocycle **20** (440 mg, 1.36 mmol) in aqueous 10% $NaHCO_3$ solution was extracted with CH_2Cl_2. The organic phase was dried over Na_2SO_4 and evaporated. The resulting oil was dissolved in CH_2Cl_2 (15 mL), treated with benzaldehyde (0.166 mL, 1.63 mmol) and $NaBH(OAc)_3$ (433 mg, 2.04 mmol), and the resulting clear solution was stirred at RT for 2 h. Water was added to the mixture and the pH was brought to basic conditions with NH_3. The mixture was extracted with CH_2Cl_2. The organic layer was dried, evaporated, and the crude residue was purified by column chromatography (eluent: petroleum ether/EtOAc 7:3) to give compound **24d** (482 mg, 94%) as a light yellow solid. ^{1}H NMR ($CDCl_3$) δ (ppm): 8.02 (d, *J* = 2.35 Hz, 1H), 7.65 (dd, *J* = 8.80, 2.35 Hz, 1H), 7.65 (d, *J* = 15.55 Hz, 1H), 7.13–7.39 (m, 5H), 7.03 (d, *J* = 8.80 Hz, 1H), 6.39 (d, *J* = 16.14 Hz, 1H), 3.82 (s, 3H), 3.71 (d, *J* = 12.91 Hz, 1H), 3.66 (d, *J* = 13.20 Hz, 1H), 2.95 (d, *J* = 16.43 Hz, 1H), 2.89 (d, *J* = 16.43 Hz, 1H), 2.80–2.97

(m, 2H), 2.63–2.80 (m, 2H), 2.26 (ddd, *J* = 13.35, 7.78, 5.28 Hz, 1H), 1.92–2.12 (m, 1H). LC–MS: (ES+) MH^+: 378.

The alkylated methyl esters **23a**, **23d–g**, **24a**, **24e–f**, **25a**, **25d–g**, **26a**, and **26d–f** were prepared analogously starting from the appropriate amine and aldehyde following the procedure for intermediate **24d** (see SI).

(±)-(E)-3-[1'-Acetyl-4-oxo-spiro(chromane-2,3'-pyrrolidine)-6-yl]-acrylic acid methyl ester (24b)

A suspension of methyl ester **20** (400 mg, 1.23 mmol) in CH_2Cl_2 (15 mL) was treated with acetyl chloride (0.105 mL, 1.49 mmol) and DIPEA (0.264 mL, 1.49 mmol) and stirred at RT for 1 h. The solution was then evaporated and the crude product was purified by chromatography column (eluent: CH_2Cl_2/MeOH 95:5) to give the 1'-acetyl derivative **24b** (240 mg, 59%) as a white solid. ^{1}H NMR ($CDCl_3$) δ (ppm): 8.06 (d, *J* = 1.76 Hz, 1H), 7.65–7.78 (m, 1H), 7.65 (d, *J* = 16.14 Hz, 1H), 7.00 (d, *J* = 8.51 Hz, 1H), 6.40 (d, *J* = 16.14 Hz, 1H), 3.82 (s, 3H), 3.34–4.13 (m, 4H), 2.82–3.12 (m, 2H), 2.29–2.57 (m, 1H), 2.11 (s, 3H), 1.87–2.09 (m, 1H); LC–MS: (ES+) MH^+: 330.

The acyl derivatives **23b–c**, **23h**, **24c**, **24h**, **25b–c**, **25h**, **26b–c** and **26h** were prepared analogously starting from the appropriate amine and acyl chloride following the procedure for intermediate **24b** (see SI).

(±)-(E)-3-[1'-(2-Phenyl-ethyl)-4-oxo-spiro[chromane-2,4'-pyrrolidine]-6-yl]-acrylic acid methyl ester (24g)

A suspension of methyl ester **20** (500 mg, 1.55 mmol) in 15 mL CH_2Cl_2 was treated with 0.33 mL DIPEA (1.86 mmol) and 0.251 mL phenethyl bromide (1.86 mmol), and stirred at RT for 8 days. The mixture was concentrated and the crude residue was purified by column chromatography (eluent: petroleum ether/EtOAc 7:3) to give methyl ester **24g** as a yellow solid (280 mg, 46%).^{1}H NMR ($CDCl_3$) δ (ppm): 8.05 (d, *J* = 2.35 Hz, 1H), 7.67 (dd, *J* = 8.80, 2.35 Hz, 1H), 7.66 (d, *J* = 15.85 Hz, 1H), 7.12–7.39 (m, 5H), 7.06 (d, *J* = 8.51 Hz, 1H), 6.40 (d, *J* = 16.14 Hz, 1H), 3.82 (s, 3H), 3.09 (d, *J* = 10.27 Hz, 1H), 2.84–3.03 (m, 4H), 2.52–2.84 (m, 5H), 2.18–2.42 (m, 1H), 1.84–2.16 (m, 1H); LC–MS: (ES+) MH^+: 392.

The 2-phenyl-ethyl derivative **26g** was prepared following the procedure for intermediate **24g** (see SI).

(±)-(E)-3-[1'-Benzyl-4-oxo-spiro(chromane-2,3'-pyrrolidine)-6-yl]-acrylic acid hydrochloride (28d)

The methyl ester **24d** (472 mg, 1.25 mmol) was then hydrolyzed in aqueous 20% HCl solution and AcOH following the procedure described for the hydrolysis of **8** giving the acrylic acid **28d** (450 mg, 90%) as a white solid (hydrochloride salt). ^{1}H NMR (DMSO–d_6, 353K) δ (ppm): 7.96 (d, *J* = 2.35 Hz, 1H), 7.93 (dd, *J* = 8.51, 2.35 Hz, 1H), 7.53–7.71 (m, 3H), 7.36–7.52 (m, 3H), 7.14 (d, *J* = 8.51 Hz, 1H), 6.44 (d, *J* = 16.14 Hz, 1H), 4.44 (d, *J* = 13.50 Hz, 1H), 4.40 (d, *J* = 13.79 Hz, 1H), 3.36–3.68 (m, 4H), 3.22 (d, *J* = 17.02 Hz, 1H), 3.10 (d, *J* = 17.02 Hz, 1H), 2.22–2.47 (m, 2H). LC–MS: (ES+) MH^+: 364.

The methyl esters **27a**, **27d–e**, **27g**, **28a–c**, **28e–h**, **29a**, **29c–d**, **30a–d** and **30g–h** were hydrolysed following the procedure for the acrylic acid **28d** (see SI), while the methyl esters **27b–c**, **27f**, **27h**, **29b**, **29e–h** and **30e–f** were prepared as described for the acrylic acid **11** (see SI).

The *N*-hydroxy-acrylamides **31a**, **31d**, **31h**, **32a-h**, **33a**, **33c**, **33d**, **33e**, **33h**, **34a-e**, and **34g-h** were prepared following the procedure for compound **16** (see SI), while the *N*-hydroxy-acrylamides **31b-c**, **31e-g**, **33b**, **33f**, **33g**, and **34f** were prepared as described for compound **15** (see SI).

(-)-(E)-3-[1'-Benzyl-4-oxo-spiro(chromane-2,3'-pyrrolidine)-6-yl]-*N*-hydroxy-acrylamide (32i)

1.89 mL (13.6 mmol) of TEA was added to solution of 1.57 g (6.81 mmol) (S)-2-(6-methoxynaphthalen-2-yl)propanoic acid in 80 mL of CH_2Cl_2. The mixture was cooled down to 0 °C, and 1.95 g (10.2 mmol) EDC and 1.38 g (10.2 mmol) HOBt were added. The mixture was stirred at 0 °C for 2 h, then the 2.20 g (6.81 mmol) acrylic acid methyl ester hydrochloric salt **20**, previously treated with 0.947 mL, (6.81 mmol) of TEA, in 20 mL CH_2Cl_2 was added and the mixture was stirred at RT overnight. The solution was washed with aqueous 5% $NaHCO_3$ solution and brine. The organic layer was then dried over Na_2SO_4 and evaporated. The crude

residue was purified by column chromatography (eluent: CH_2Cl_2/*i*-PrOH 99:1) and the 6-methoxynaphthalen-2-yl diastereoisomers **35** and **36** were separated. The less polar isomer was re-crystallized from *i*-PrOH to give 980 mg (29%) of (+)-acrylic acid methyl ester **35** as a white solid. ^{1}H NMR ($CDCl_3$) δ (ppm): 8.01 (d, *J*=2.35 Hz, 1 H), 7.48-7.82 (m, 5 H), 7.38 (ddd, *J*=10.78, 8.73, 1.61 Hz, 1 H), 7.10-7.25 (m, 2 H), 7.01 and 6.59 (d, *J*=8.51 Hz, 1 H), 6.41 (d, *J*=16.14 Hz, 1 H), 4.02-4.17 (m, 1 H), 3.96 (s, 3 H), 3.82 (s, 3 H), 3.65-3.91 (m, 3 H), 3.28-3.57 (m, 1 H), 2.95 and 2.79 (d, *J*=16.73 Hz, 1 H), 2.86 (d, *J*=16.73 Hz, 1 H), 2.15-2.39 (m, 1 H), 1.69-2.15 (m, 1 H), 1.56 (d, *J*=6.16 Hz, 3 H); LC-MS: (ES+) MH^+: 500; optical rotation: α_D= +5.9°, c=1.025 g/100 mL in CH_2Cl_2. 926 mg (1.85 mmol) of the methyl ester **35** suspended in 5 mL of glacial AcOH, was then treated with 5 mL (30 mmol) of 20% aqueous HCl. The mixture was stirred in the microwave oven at 120°C for 3 h. 5 mL of water was added and the reaction mixture was extracted three times with CH_2Cl_2. The aqueous phase was evaporated, then 25 mL of methanol and a catalytic amount of H_2SO_4 were added and the mixture was heated to reflux overnight. The solution was poured into water and NH_3 was added to adjust the pH to 9-10. The aqueous phase was extracted with CH_2Cl_2, dried over Na_2SO_4, filtered, and the solvent was evaporated to give the (+)-oxo-spiro(chromane-2,3'-pyrrolidine) methyl ester **37** (210 mg, 39.5%) as a yellow oil (free base). ^{1}H NMR (DMSO-d_6) δ (ppm): 7.99 (d, *J*=2.05 Hz, 1H), 7.96 (dd, *J*=8.51, 2.35 Hz, 1 H), 7.67 (d, *J*=16.14 Hz, 1 H), 7.06 (d, *J*=8.51 Hz, 1 H), 6.56 (d, *J*=16.14 Hz, 1 H), 3.72 (s, 3 H), 2.74-3.10 (m, 6 H), 1.88-2.10 (m, 1 H), 1.65-1.85 (m, 1 H); LC-MS: (ES+) MH^+: 288; optical rotation: α_D= +1.97°, c=0.72 g/100 mL in CH_2Cl_2.

180 mg (0.63 mmol) of the methyl ester **37** was then treated with benzaldehyde and $NaBH(OAc)_3$ according to the procedure used for compound **24d** to give 180 mg (76%) of the (+)-(E)-3-[1'-benzyl-4-oxo-spiro(chromane-2,3'-pyrrolidine)-6-yl]-acrylic acid methyl ester [^{1}H NMR (DMSO-d_6) δ (ppm): 7.97 (d, *J*=2.35 Hz, 1 H), 7.97 (dd, *J*=9.39, 2.35 Hz, 1 H), 7.66 (d, *J*=16.14 Hz, 1 H), 7.17-7.35 (m, 5 H), 7.10 (d, *J*=9.10 Hz, 1 H), 6.56 (d, *J*=16.14 Hz, 1 H), 3.72 (s, 3 H), 3.61 (s, 2 H), 2.91-3.04 (m, 2 H), 2.69-2.89 (m, 2 H), 2.53-2.67 (m, 2 H), 1.86-2.21 (m, 2 H); LC-MS: (ES+) MH^+: 378; Optical rotation: α_D=+1.68°, c=0.96 g/100 mL in CH_2Cl_2)], which was first hydrolyzed using aqueous HCl (20%) solution and AcOH following the procedure described for compound **12** giving 120 mg (88%) of the corresponding acrylic acid as its hydrochloride salt and as a white solid [^{1}H NMR (DMSO-d_6) δ (ppm): 11.01-11.75 (m, 1 H), 7.91-8.12 (m, 2 H), 7.53-7.71 (m, 3 H), 7.37-7.53 (m, 3 H), 6.95-7.26 (m, 1 H), 6.30-6.57 (m, 1

H), 4.29-4.58 (m, 2 H), 2.91-3.67 (m, 6 H), 1.98-2.45 (m, 2 H); LC-MS: (ES+) MH^+: 364; Optical rotation: α_D= -3.4°, c=0.43 g/100 mL in MeOH)], and then treated with NH_2OTHP following the procedure described for compound **16** giving 80 mg (63%) of the *N*-(tetrahydro-pyran-2-yloxy)-acrylamide as a light yellow solid [^{1}H NMR (DMSO-d_6) δ (ppm): 11.13 (bs, 1 H), 7.90 (d, *J*=2.05 Hz, 1 H), 7.67-7.84 (m, 1 H), 7.47 (d, *J*=15.85 Hz, 1 H), 7.16-7.39 (m, 5 H), 7.10 (d, *J*=8.80 Hz, 1 H), 6.46 (d, *J*=16.14 Hz, 1 H), 4.79-5.00 (m, 1 H), 3.86-4.10 (m, 1 H), 3.62 (s, 2 H), 3.47-3.58 (m, 1 H), 3.01 (d, *J*=17.02 Hz, 1 H), 2.95 (d, *J*=17.02 Hz, 1 H), 2.55-2.88 (m, 4 H), 1.88-2.18 (m, 2 H), 1.47-1.83 (m, 6 H); LC-MS: (ES+) MH^+: 463]. The THP protected hydroxamic acid was then hydrolyzed according to the procedure for compound **16** giving 31.3 mg (44%) of the requisite hydroxamic acid **32i** as its hydrochloride salt. ^{1}H NMR (DMSO-d_6) δ (ppm): 7.92 (d, *J*=2.35 Hz, 1 H), 7.80 (dd, *J*=8.36, 2.49 Hz, 1 H), 7.34-7.61 (m, 6 H), 7.12 (d, *J*=8.22 Hz, 1 H), 6.51 (d, *J*=16.14 Hz, 1 H), 4.34 (bs, 2 H), 3.11-3.53 (m, 6 H), 2.29-2.44 (m, 2 H); optical rotation: α_D= -4.4°, c=0.27 g/100 mL in MeOH; LC-MS: Method F, rt=1.22; (ES+) MH^+: 379.

The synthesis of (+)-(E)-3-[1'-benzyl-4-oxo-spiro(chromane-2,3'-pyrrolidine)-6-yl]-*N*-hydroxy-acrylamide (**32j**) is disclosed in the supplementary information.

(-)-(E)-3-[1'-Benzyl-4-oxo-spiro(chromane-2,3'-piperidine)-6-yl]-*N*-hydroxy-acrylamide (33i)

5 mL of 4 M HCl in dioxane was added to a solution of 2.50 g (6.31 mmol) of intermediate **5** dissolved in 20 mL of CH_2Cl_2. The mixture was stirred for 5 h at RT and the resulting precipitate was collected by filtration to give 2.079 g (89%) of (±)-6-bromospiro[chroman-2,3'-piperidin]-4-one hydrochloride.^{1}H NMR (DMSO-d_6) δ (ppm): 9.69 (bs, 1H), 8.83 (bs, 1 H), 7.82 (d, *J*=2.93 Hz, 1H), 7.80 (dd, *J*=6.75, 2.64 Hz, 1H), 7.11 (d, *J*=9.10 Hz, 1H), 3.39-3.54 (m, 1H), 3.10-3.26 (m, 2H), 3.00 (d, *J*=17.02 Hz, 1H), 2.86 (d, *J*=17.31 Hz, 1H), 2.62-2.86 (m, 1 H), 1.98-2.18 (m, 1H), 1.78-1.98 (m, 1H), 1.56-1.78 (m, 2H); LC-MS: 297. 1.577 mL (11.32 mmol) of TEA, 1.085 g (5.66 mmol) of EDC and 0.866 g (5.62 mmol) of HOBt·H_2O were added to a solution of 0.732 g (3.77 mmol) of (R)-2-acetoxy-2-phenylacetic acid in 50 mL CH_2Cl_2 and the mixture was stirred at RT for 10 min. Then, 1.39 g (4.12 mmol) of the racemic spiropiperidine intermediate was added and the mixture was stirred at RT for 18 h. After washing with 5% $NaHCO_3$ and with

brine the organic layer was dried over Na_2SO_4 and evaporated to dryness. The crude mixture of diastereoisomers was purified by silica gel chromatography (eluent: petroleum ether/EtOAc from 6:4 to 3:7). The less polar isomer that eluted first (430 mg, 22%, ^{1}H NMR (DMSO-d_6) δ (ppm): 7.68-7.83 (m, 2H), 7.19-7.65 (m, 5H), 6.94 (d, *J*=8.80 Hz, 1H), 6.38 (s, 1H), 4.11 (d, *J*=13.50 Hz, 1H), 3.45-3.87 (m, 1H), 2.88-3.19 (m, 2H), 2.77 (d, *J*=17.02 Hz, 1H), 2.67 (d, *J*=17.02 Hz, 1H), 2.10 (s, 3H), 1.36-2.02 (m, 3H), 1.00-1.32 (m, 1H)) was then dissolved in 25 mL of EtOH and 25 mL of 12 M HCl. The resulting mixture was stirred at reflux overnight. Then EtOH was evaporated and the residue was brought to basic pH with 20% NaOH and extracted with EtOAc. The organic phase was dried over Na_2SO_4 and evaporated to dryness to give 216 mg (80%) of the (-)-6-bromospiropiperidin intermediate **39**.^{1}H NMR (DMSO-d_6) δ (ppm): 7.76 (d, *J*=2.35 Hz, 1H), 7.71 (dd, *J*=8.51, 2.64 Hz, 1H), 7.04 (d, *J*=8.80 Hz, 1H), 2.91 (d, *J*=16.73 Hz, 1H), 2.78 (d, *J*=17.02 Hz, 1H), 2.74-2.90 (m, 2H), 2.65-2.74 (m, 1H), 2.54-2.64 (m, 1H), 1.80-1.90 (m, 1H), 1.52-1.79 (m, 2H), 1.31-1.47 (m, 1H); optical rotation: α_D= -19.28°, c=0.5 g/100 mL in MeOH (hydrochloride salt).

798 mg (2.69 mmol) of the (-)-6-bromospirochroman intermediate **39** was dissolved in 30 mL of CH_2Cl_2. 0.939 mL (6.74 mmol) TEA and 588 mg (2.69 mmol) BOC anhydride were added and the solution was stirred overnight at RT and was then washed with 5% citric acid followed by 5% $NaHCO_3$. The organic layer was dried over Na_2SO_4 and evaporated to dryness. The crude product was purified by column chromatography (eluent: petroleum ether/EtOAc 6:4, v:v) to give 1.00 g (94%) of the *tert*-butyl ester **41**. ^{1}H NMR (DMSO-d_6) δ (ppm): 7.79 (d, *J*=2.35 Hz, 1H), 7.74 (d, *J*=8.22 Hz, 1H), 6.67-7.10 (m, 1H), 3.59-3.99 (m, 2H), 2.61-3.18 (m, 4H), 1.90-2.07 (m, 1H), 1.63-1.83 (m, 2H), 1.48-1.55 (m, 1H), 1.47 (s, 9H); LC-MS: (ES+) 395; optical rotation: α_D = +20.67°, c=0.505 g/100 mL in MeOH.

587 mg (6.81 mmol) of methyl acrylate and 0.950 mL (6.81 mmol) of TEA were added to a solution of 900 mg (2.27 mmol) of intermediate **41** in 3 mL DMF and the mixture was degassed with nitrogen. 27.7 mg (0.091 mmol) $P(o\text{-}tol)_3$ and 10.2 mg (0.045 mmol) $Pd(OAc)_2$ were added and the mixture was heated at 100 °C under nitrogen for 3 h. Further $Pd(OAc)_2$ (10.2 mg, 0.045 mmol) was added and the solution was heated for additional 5 h and then partitioned between Et_2O and water. The aqueous phase was washed with Et_2O and the collected organic layer were washed with water, dried over Na_2SO_4 and evaporated to dryness. The crude product was purified by column chromatography (eluent: petroleum ether: EtOAc 9:1 to 7:3) to give 734 mg

(81%) of (+)-*tert*-butyl 6-[(E)-3-methoxy-3-oxo-prop-1-enyl]-4-oxo-spiro[chromane-2,3'-piperidine]-1'-carboxylate. ^{1}H NMR (DMSO-d_6) δ (ppm): 7.89-8.09 (m, 2H), 7.68 (d, *J*=16.14 Hz, 1H), 6.97-7.09 (m, 1H), 6.57 (d, *J*=16.14 Hz, 1H), 3.75-4.03 (m, 2H), 3.72 (s, 2H), 2.62-3.21 (m, 3H), 2.03 (bs, 1H), 1.65-1.87 (m, 2H), 1.28-1.62 (m, 3H), 1.00-1.26 (m, 9H); LC-MS: (ES+) 402; optical rotation: α_D = +22.40 c=0.25 g/100 mL in MeOH. 710 mg (1.77 mmol) of the acrylic acid methyl ester was dissolved in 50 mL CH_2Cl_2. 2 mL of 4 M HCl in dioxane was added and the mixture was stirred at RT for 3 h. The precipitate was filtered, washed with CH_2Cl_2 and dried to give 516 mg (86%) of the free amine intermediate as its hydrochloride salt [^{1}H NMR (DMSO-d_6) δ (ppm): 9.08 (bs, 2H), 8.05 (dd, *J*=8.80, 2.35 Hz, 1H), 8.02 (d, *J*=2.35 Hz, 1H), 7.69 (d, *J*=16.14 Hz, 1H), 7.15 (d, *J*=8.51 Hz, 1H), 6.59 (d, *J*=16.14 Hz, 1H), 3.73 (s, 3H), 3.42-3.56 (m, 1H), 3.13-3.27 (m, 2H), 3.02 (d, *J*=17.02 Hz, 1H), 2.86 (d, *J*=16.73 Hz, 1H), 2.78-2.88 (m, 1H), 1.59-2.11 (m, 4H); LC-MS: (ES+) 302; optical rotation: α_D = -43.67 c=0.24 g/100 mL in MeOH], which was then converted with benzaldehyde and $NaBH(OAc)_3$ according to the procedure used for compound **24d** into the *N*-benzyl analogue (547 mg, 93%).^{1}H NMR (DMSO-d_6) δ (ppm): 7.98 (dd, *J*=8.80, 2.35 Hz, 1H), 7.90 (d, *J*=2.05 Hz, 1H), 7.65 (d, *J*=16.14 Hz, 1H), 7.14-7.28 (m, 5H), 7.10 (d, *J*=8.51 Hz, 1H), 6.54 (d, *J*=16.14 Hz, 1H), 3.72 (s, 3H), 3.53 (d, *J*=13.79 Hz, 1H), 3.45 (d, *J*=13.79 Hz, 1H), 2.96 (d, *J*=16.73 Hz, 1H), 2.89 (d, *J*=16.73 Hz, 1H), 2.53-2.59 (m, 1H), 2.38-2.46 (m, 3H), 1.65-1.91 (m, 3H), 1.41-1.61 (m, 1H); LC-MS: (ES+) 392; optical rotation: α_D = -29.92 c=0.26 g/100 mL in MeOH. Hydrolysis of 525 mg (1.34 mmol) of the methyl ester according to the procedure for compound **11** gave 435 mg (86%) of the corresponding acrylic acid [^{1}H NMR (DMSO-d_6) δ (ppm): 12.29 (s, 1H), 7.94 (dd, *J*=8.66, 2.20 Hz, 1H), 7.86 (d, *J*=2.05 Hz, 1H), 7.57 (d, *J*=16.14 Hz, 1H), 7.15-7.29 (m, 5H), 7.09 (d, *J*=8.80 Hz, 1H), 6.43 (d, *J*=15.85 Hz, 1H), 3.53 (d, *J*=14.09 Hz, 1H), 3.45 (d, *J*=14.09 Hz, 1H), 2.96 (d, *J*=16.73 Hz, 1H), 2.89 (d, *J*=17.02 Hz, 1H), 2.54-2.61 (m, 1H), 2.33-2.46 (m, 3H), 1.69-1.93 (m, 3H), 1.48-1.65 (m, 1H); LC-MS: (ES+) 378; optical rotation: α_D = -18.96 c=0.25 g/100 mL in MeOH], which was then converted following the procedure described for compound **16** into the requisite hydroxamic acid **33i**, that was purified by trituration in *i*-PrOH (81.5 mg, 18%, hydrochloride salt). ^{1}H NMR (DMSO-d_6) δ (ppm): 10.71 (bs, 1H), 10.21 (bs, 1H), 7.78-8.12 (m, 2H), 7.35-7.76 (m, 6H), 7.25 (d, *J*=8.51 Hz, 1H), 6.44 (d, *J*=15.55 Hz, 1H), 4.36-4.53 (m, 1H), 4.26 (dd, *J*=12.91, 5.58 Hz, 1H), 3.46-3.59 (m, 2H), 3.10-3.28 (m, 1H), 2.99 (d, *J*=17.02 Hz, 1H), 2.86-2.95 (m, 1H), 2.79 (d, *J*=17.02 Hz, 1H), 1.87-2.18 (m, 2 H), 1.71-1.87 (m, 1H), 1.51-

1.71 (m, 1H); LC-MS: Method C, rt=3.11; (ES+) MH^+: 393; optical rotation: α_D = -12.30 c= 1 g/100 mL in MeOH.

The synthesis of (+)-(E)-3-[1'-benzyl-4-oxo-spiro(chromane-2,3'-piperidine)-6-yl]-*N*-hydroxy-acrylamide **(33j)** is disclosed in the supplementary information.

4.2 Biological Assays.

4.2.1 HDACs Inhibition Assay

The *in vitro* activity of HDAC inhibitors was assayed using the HDAC fluorescent histone deacetylase activity assay kit (Biomol Research Laboratories, Plymouth Meeting, PA). In specific, 15 μL of a nuclear extract from HeLa cells was diluted to 50 μL with the assay buffer containing the HDAC inhibitor and a peptide containing acetylated lysine as substrate at a concentration of 200 μM. The samples were incubated for 15 min at room temperature and then exposed to a developer for a further 10 min. Substrate fluorescence was measured using an excitation at 355 nm and emission at 460 nm, and the % inhibition was calculated relative to untreated samples. In order to eliminate possible background interferences the fluorescence was measured for each compound at the test concentrations in the assay buffer in absence of the enzyme. IC_{50} values were determined using a non-linear regression analysis of the concentration/inhibition data.

The in vitro activities of recombinant human HDACs 2, 3 and 6 (BPS Bioscience, San Diego, CA) were assessed using a fluorescent substrate (AK500, Biomol Research Laboratories, Plymouth Meeting, PA). 6.5 μL of the recombinant HDAC proteins (which corresponds to 20 μg/well, 6 μg/well and 500 μg/well for HDACs 2, 3, and 6, respectively) were diluted to 25 μL with the assay buffer containing the HDAC inhibitors and 25 μM of the substrate. The samples were incubated for 15 min at room temperature and then exposed to a developer for another 10 min.

4.2.2 Immunoblots and Antibodies

Whole cell extracts were obtained by lysis in buffer supplemented with proteases inhibitors (20 mM Tris HCl pH 7.5, 25% glycerol, 420 mM NaCl, 15 mM $MgCl_2$, 0.2 mM EDTA, 0.1% NP40). Proteins were separated by SDS-PAGE, blotted onto PVDF membranes and probed with the indicated antibodies. The employed antibodies were anti-HDAC1, anti-HDAC3, anti-HDAC4, anti-HDAC5 and anti-HDAC6 (Cell Signaling, Leiden, The Netherlands), anti-HDAC2 (Abcam, Cambridge, UK) and anti α-tubulin (Sigma-Aldrich, Milan, Italy). Horseradish peroxidase–conjugated secondary antibodies (Sigma-Aldrich, Milan, Italy) were used with enhanced chemiluminescence (Amersham Pharmacia Biotech) for detection.

4.2.3 Cell Growth Assay

The effect of the HDAC inhibitors on cell proliferation was evaluated against K562 (chronic myeloid carcinoma), A549 (non-small-cell lung cancer) and HCT-116 (human colon cancer) tumor cell lines using the CellTiter–Glo Luminescent Cell Viability Assay (Promega, Madison, WI, USA) according to the manufacturer's instructions. K562, A549 and HCT–116 cells were first incubated for 72 h with the inhibitors at different concentrations. Then, an equivalent of the CellTiter–Glo reagent was added, the solution was mixed for 2 min in order to induce cell lysis, and the luminescence was recorded after another 10 min. The IC_{50} was calculated using GraphPad Software.

4. 2.4 Molecular Modeling

Target Preparation

The protein structures of the catalytic domain of HDAC1 and HDAC2, pdb identifiers 4BKX [35] and 4LXZ[36], respectively, were prepared for docking with Autodock[43] and Plants[44] as well as a for a final optimization with Mopac[45]. The pdb files of the structures were downloaded from the Protein Data Bank (www.rcsb.org) and prepared with same multi-step procedure here described. In Chimera software[46] the HDAC proteins, the zinc ions and the ligands (vorinostat in 4LXZ and the acetate in 4BKX) were kept while the other molecules were removed. Hydrogen atoms were added to the residues and optimized for the *H*-bonding networks

both automatically (Chimera defaults) and manually (for glutamine, asparagine and histidine residues). In particular, the histidine 140 (numbering according to the human HDAC1 sequence Uniprot identifier Q13547 or HDAC1_HUMAN) was considered protonated based on the interaction with the hydroxamic group of the ligand.[38, 47] Then, hydrogens were optimized for positions with a 100 Steepest Descent minimization. Both structures were then energetically optimized at Semi-empirical Quantum Mechanics (SQM) level of theory in Mopac software; with localized molecular orbital method (MOZYME), PM7[48] as Hamiltonian and the Conductor-like Screening Model (COSMO)[49] to simulate the water environment. Firstly, the Lewis structure was properly assigned and the positions of the hydrogen atoms were minimized till a gradient norm of 50 kcal/mol/Å. Then, all the atoms of the complexes were geometrically optimized for 50 cycles. The resulting structures were used to create the input files for Autodock and Plants. Partial charges for the proteins were assigned by Chimera based on the Amber ff12SB Force Field. In addition, the Zn ion was modelled with charge +1 as calculated at the SQM optimization step. The two proteins were superposed onto each other and an area of 15 Angstroms around the geometrical centre of the vorinostat ligand in HDAC2 was considered for the binding site. Finally, the grid maps necessary for Autodock docking were generated with Autogrid software.

Docking Procedure

After several docking trials with Autodock and Plants a two stages protocol was selected to explore the ligand binding against the 2 HDAC proteins. First, the common substructure of the ligands presented in this study (the hydroxamic group linked to the chromane ring system) was placed, by means of the rigid protocol in Autodock, into to the binding site. This part has a high degree of delocalized electrons resulting in a rigid and planar structure. Afterwards, the rest of the molecule was added to the putative complex using Plants with the function 'shape_constraint' which uses a specified three-dimensional structure to constrain the volume occupied by the ligand in that protein region. Based on the scores and the visual inspection of the docking poses the best solutions were selected for the following optimization. The hydroxamic acid moiety of the studied ligands was modelled always in its basic, deprotonated form (hydroxamate) as suggested by various studies on the Zn binding groups.[32, 47]

Optimization and Scoring

Class I HDAC proteins are zinc-dependent enzymes, the metal is used to catalyse the reaction and to bind both, the protein and the ligand. Because no explicit electrons are described in Molecular Mechanics (MM), this level of theory has limitations in representing the nature of these ligand-enzyme complexes. Thus, although certain modifications to MM were suggested[50], we used the Semi-empirical Quantum Mechanics to optimize the interactions of the studied complexes. The best hypotheses of binding predicted at the docking step for the investigated molecules were optimized, in SQM till a gradient norm of 10 kcal/mol/Å, inside the fixed and previously treated target structure (see target preparation), with the MOZYME method, PM7 Hamiltonian, COSMO solvent model and with the EF routine.[51] Finally, the energy for each complex is estimated by subtracting the heat of formations of the target and the ligand alone from the one of the complex. This is a rough estimate of the energy gained by the interaction but gives an indication for comparing the strength of binding of similar molecules.

The graphical representations of the coordinates of the protein-ligand complexes were created with PyMOL[52]. The hydrophobic favorable interaction areas are derived from exploration of the interaction energy, in protein regions, with an aliphatic carbon atom as probe by means of Autogrid software for Autodock. In the figure the surface representation of the grid points with energy value smaller than -0.25 kcal/mol was done with the Autodock plugin for PyMOL.[53]

4. 2.5 Metabolic Stability in Hepatic Microsomes

The inhibitors at 1 μM concentration were pre-incubated for 10 min at 37 °C in potassium phosphate buffer (pH 7.4) together with 0.5 mg/mL mouse or human hepatic microsomes (Xenotech, Kansas City, USA). The cofactor mixture including NADP, G6P and G6P-DH was added and aliquots were taken after 0 and 30 min. The samples were analyzed on an Acquity UPLC, coupled with a Sample Organizer and interfaced with a triple quadrupole Premiere XE (Waters, Milford, USA). Mobile phases consisted of a phase A [0.1% formic acid in a mixture of water and acetonitrile (95:5, v:v)] and phase B [0.1% formic acid in a mixture of water and acetonitrile (5:95, v:v)]. Separations were carried out at 40 °C on Acquity BEH C18 columns (50mm×2.1mm×1.7μm, flow rate of 0.45 mL/min or 50mm×1mm×1.7μm, flow rate of 0.2

mL/min). The column was conditioned with 2% of Phase B for 0.2 min, then brought to 100% of Phase B within 0.01 min and maintained at these conditions for 1.3 min. The operating parameters of the MS were set as follows: capillary voltage 3.4 kV, source temperature 115 °C, desolvation temperature 450 °C, desolvation gas flow 900 L/h, cell pressure 3.3×10^{-3} mbar. Cone voltage and collision energy were optimized for every compound. LC-MS/MS analyses were performed using a positive electrospray ionisation (ESI^+) interface in MRM (multiple reaction monitoring) mode with verapamil as internal standard. The percentage of the compound remaining after 30 min incubation was calculated according the following equation: [area at time 30 min]/ [area at time 0 min]*100%.

4. 2.6 Inhibition of Human CYP450 Isoenzymes Activity

The cytochrome P450 inhibition experiments were carried out by adapting previously described protocols [54, 55] and following the manufacturer's instructions (BD Biosciences, New Jersey, USA). The compounds were dissolved in a 96-well plate at 10 μM concentration in a potassium phosphate buffer (pH 7.4) containing a NADPH regenerating system. The final cofactor concentrations were 1.3 mM $NADP^+$, 3.3 mM glucose 6-phosphate and 0.4 U/ml glucose-6-phosphate dehydrogenase for all enzyme/substrate pairs. The reaction was initiated by adding the specific isoenzymes (Supersomes, Gentest) and substrates at 37 °C. Furafylline (for CYP1A2, 100 μM), tranylcypromine (for CYP2C19, 500 μM), quinidine (for CYP2D6, 0.5 μM), and ketoconazole (for CYP3A4, 1.66 μM) were employed as control inhibitors. Incubations were carried out for 15 min (0.5 pmol CYP1A2, 5 μM 3-cyano-7-ethoxycoumarin (CEC)), 30 min (0.5 pmol CYP2C19, 25 μM CEC; 1 pmol CYP3A4, 50 μM 7-benzyloxy-4-(trifluoromethyl)-coumarin; 1.5 pmol CYP2D6, 1.5 μM 3-[2-(*N*,*N*-diethyl-*N*-methylamino)ethyl]-7-methoxy-4-methylcoumarin). The reaction was stopped by adding 75 μL of a mixture of 80% acetonitrile and 20% 0.5 M TRIS base and the plates were read on a fluorimeter at the appropriate emission/excitation wavelengths.[55] The percentage of inhibition was calculated relative to enzyme samples without inhibitors.

Supplementary data. Synthesis and characterization of prepared compounds. HPLC purity of the obtained hydroxamic acid derivatives. This material is available free of charge via the Internet.

References

[1] E.I. Campos, D. Reinberg, Histones: Annotating Chromatin, Annu. Rev. Genet., 43 (2009) 559-599.

[2] M. Simon, J.A. North, J.C. Shimko, R.A. Forties, M.B. Ferdinand, M. Manohar, M. Zhang, R. Fishel, J.J. Ottesen, M.G. Poirier, Histone fold modifications control nucleosome unwrapping and disassembly, Proc Natl Acad Sci U S A, 108 (2011) 12711-12716.

[3] C.M. Grozinger, C.A. Hassig, S.L. Schreiber, Three proteins define a class of human histone deacetylases related to yeast Hda1p, Proc Natl Acad Sci U S A, 96 (1999) 4868-4873.

[4] S.G. Gray, T.J. Ekstrom, The human histone deacetylase family, Exp Cell Res, 262 (2001) 75-83.

[5] H.Y. Lin, C.S. Chen, S.P. Lin, J.R. Weng, Targeting histone deacetylase in cancer therapy, Med. Res. Rev., 26 (2006) 397-413.

[6] R. Ficner, Novel structural insights into class I and II histone deacetylases, Curr Top Med Chem, 9 (2009) 235-240.

[7] E. Verdin, F. Dequiedt, H.G. Kasler, Class II histone deacetylases: versatile regulators, Trends Genet, 19 (2003) 286-293.

[8] X.J. Yang, S. Gregoire, Class II histone deacetylases: from sequence to function, regulation, and clinical implication, Mol Cell Biol, 25 (2005) 2873-2884.

[9] F. Thaler, C. Mercurio, Towards selective inhibition of histone deacetylase isoforms: what has been achieved, where we are and what will be next, ChemMedChem, 9 (2014) 523-536.

[10] K. Huber, G. Superti-Furga, After the grape rush: sirtuins as epigenetic drug targets in neurodegenerative disorders, Bioorg Med Chem, 19 (2011) 3616-3624.

[11] S. Spange, T. Wagner, T. Heinzel, O.H. Kramer, Acetylation of non-histone proteins modulates cellular signalling at multiple levels, Int. J. Biochem. Cell Biol., 41 (2009) 185-198.

[12] M. Ocker, Deacetylase inhibitors - focus on non-histone targets and effects, World J Biol Chem, 1 (2010) 55-61.

[13] S. Minucci, P.G. Pelicci, Histone deacetylase inhibitors and the promise of epigenetic (and more) treatments for cancer, Nat. Rev. Cancer, 6 (2006) 38-51.

[14] M. Paris, M. Porcelloni, M. Binaschi, D. Fattori, Histone deacetylase inhibitors: from bench to clinic, J. Med. Chem., 51 (2008) 1505-1529.

[15] A.G. Kazantsev, L.M. Thompson, Therapeutic application of histone deacetylase inhibitors for central nervous system disorders, Nat. Rev. Drug Discov., 7 (2008) 854-868.

[16] R. Glauben, E. Sonnenberg, M. Zeitz, B. Siegmund, HDAC inhibitors in models of inflammation-related tumorigenesis, Cancer Lett., 280 (2009) 154-159.

[17] F. Thaler, S. Minucci, Next generation histone deacetylase inhibitors: the answer to the search for optimized epigenetic therapies?, Expert Opin. Drug Disc., 6 (2011) 393-404.

[18] M. Federico, L. Bagella, Histone deacetylase inhibitors in the treatment of hematological malignancies and solid tumors, J Biomed Biotechnol, 2011 (2011) 475641.

[19] J.S. Graham, S.B. Kaye, R. Brown, The promises and pitfalls of epigenetic therapies in solid tumours, Eur J Cancer, 45 (2009) 1129-1136.

[20] C. Mercurio, S. Minucci, P.G. Pelicci, Histone deacetylases and epigenetic therapies of hematological malignancies, Pharmacol. Res., 62 (2010) 18-34.

[21] A. Petrella, B. Fontanella, A. Carratu, V. Bizzarro, M. Rodriquez, L. Parente, Histone deacetylase inhibitors in the treatment of hematological malignancies, Mini Rev Med Chem, 11 (2011) 519-527.

[22] P.A. Marks, Discovery and development of SAHA as an anticancer agent, Oncogene, 26 (2007) 1351-1356.

[23] R.L. Piekarz, R. Frye, M. Turner, J.J. Wright, S.L. Allen, M.H. Kirschbaum, J. Zain, H.M. Prince, J.P. Leonard, L.J. Geskin, C. Reeder, D. Joske, W.D. Figg, E.R. Gardner, S.M. Steinberg, E.S. Jaffe, M. Stetler-Stevenson, S. Lade, A.T. Fojo, S.E. Bates, Phase II multi-institutional trial of the histone deacetylase inhibitor romidepsin as monotherapy for patients with cutaneous T-cell lymphoma, J Clin. Oncol., 27 (2009) 5410-5417.

[24] S. Jain, J. Zain, Romidepsin in the treatment of cutaneous T-cell lymphoma, J Blood Med, 2 (2011) 37-47.

[25] K.M. VanderMolen, W. McCulloch, C.J. Pearce, N.H. Oberlies, Romidepsin (Istodax, NSC 630176, FR901228, FK228, depsipeptide): a natural product recently approved for cutaneous T-cell lymphoma, J Antibiot (Tokyo), 64 (2011) 525-531.

[26] R.M. Poole, Belinostat: first global approval, Drugs, 74 (2014) 1543-1554.

[27] A. Bodiford, M. Bodge, M.S. Talbott, N.M. Reddy, Profile of belinostat for the treatment of relapsed or refractory peripheral T-cell lymphoma, Onco Targets Ther, 7 (2014) 1971-1977.

[28] K.P. Garnock-Jones, Panobinostat: First Global Approval, Drugs, 75 (2015) 695-704.

[29] J.H. Lee, M.L. Choy, P.A. Marks, Mechanisms of resistance to histone deacetylase inhibitors, Adv Cancer Res, 116 (2012) 39-86.

[30] M. Varasi, F. Thaler, A. Abate, C. Bigogno, R. Boggio, G. Carenzi, T. Cataudella, R. Dal Zuffo, M.C. Fulco, M.G. Rozio, A. Mai, G. Dondio, S. Minucci, C. Mercurio, Discovery,

synthesis, and pharmacological evaluation of spiropiperidine hydroxamic acid based derivatives as structurally novel histone deacetylase (HDAC) inhibitors, J. Med. Chem., 54 (2011) 3051-3064.

[31] T.A. Miller, D.J. Witter, S. Belvedere, Histone deacetylase inhibitors, J. Med. Chem., 46 (2003) 5097-5116.

[32] P. Bertrand, Inside HDAC with HDAC inhibitors, Eur J Med Chem, 45 (2010) 2095-2116.

[33] F. Thaler, M. Varasi, G. Carenzi, A. Colombo, A. Abate, C. Bigogno, R. Boggio, S. Carrara, T. Cataudella, R. Dal Zuffo, V. Reali, S. Vultaggio, G. Dondio, S. Gagliardi, S. Minucci, C. Mercurio, Spiro[chromane-2,4'-piperidine]-based histone deacetylase inhibitors with improved in vivo activity, ChemMedChem, 7 (2012) 709-721.

[34] L. Yang, G. Morriello, K. Prendergast, K. Cheng, T. Jacks, W.W. Chan, K.D. Schleim, R.G. Smith, A.A. Patchett, Potent 3-spiropiperidine growth hormone secretagogues, Bioorg. Med. Chem. Lett., 8 (1998) 107-112.

[35] C.J. Millard, P.J. Watson, I. Celardo, Y. Gordiyenko, S.M. Cowley, C.V. Robinson, L. Fairall, J.W. Schwabe, Class I HDACs share a common mechanism of regulation by inositol phosphates, Mol Cell, 51 (2013) 57-67.

[36] B.E. Lauffer, R. Mintzer, R. Fong, S. Mukund, C. Tam, I. Zilberleyb, B. Flicke, A. Ritscher, G. Fedorowicz, R. Vallero, D.F. Ortwine, J. Gunzner, Z. Modrusan, L. Neumann, C.M. Koth, P.J. Lupardus, J.S. Kaminker, C.E. Heise, P. Steiner, Histone deacetylase (HDAC) inhibitor kinetic rate constants correlate with cellular histone acetylation but not transcription and cell viability, J Biol Chem, 288 (2013) 26926-26943.

[37] D.P. Dowling, S.L. Gantt, S.G. Gattis, C.A. Fierke, D.W. Christianson, Structural studies of human histone deacetylase 8 and its site-specific variants complexed with substrate and inhibitors, Biochemistry, 47 (2008) 13554-13563.

[38] K. Vanommeslaeghe, S. Loverix, P. Geerlings, D. Tourwe, DFT-based ranking of zinc-binding groups in histone deacetylase inhibitors, Bioorg Med Chem, 13 (2005) 6070-6082.

[39] J. Zhou, H. Xie, Z. Liu, H.B. Luo, R. Wu, Structure-function analysis of the conserved tyrosine and diverse pi-stacking among class I histone deacetylases: a QM (DFT)/MM MD study, J Chem Inf Model, 54 (2014) 3162-3171.

[40] F. Thaler, A. Colombo, A. Mai, R. Amici, C. Bigogno, R. Boggio, A. Cappa, S. Carrara, T. Cataudella, F. Fusar, E. Gianti, S. Joppolo di Ventimiglia, M. Moroni, D. Munari, G. Pain, N. Regalia, L. Sartori, S. Vultaggio, G. Dondio, S. Gagliardi, S. Minucci, C. Mercurio, M. Varasi, Synthesis and biological evaluation of *N*-hydroxyphenylacrylamides and *N*-hydroxypyridin-2-ylacrylamides as novel histone deacetylase inhibitors, J. Med. Chem., 53 (2010) 822-829.

[41] F. Thaler, A. Colombo, A. Mai, C. Bigogno, R. Boggio, S. Carrara, S. Joppolo di Ventimiglia, D. Munari, N. Regalia, G. Dondio, S. Gagliardi, S. Minucci, C. Mercurio, M. Varasi, Synthesis and biological characterization of amidopropenyl-hydroxamates as HDAC inhibitors, ChemMedChem, 5 (2010) 1359-1372.

[42] F. Thaler, M. Varasi, A. Abate, G. Carenzi, A. Colombo, C. Bigogno, R. Boggio, R.D. Zuffo, D. Rapetti, A. Resconi, N. Regalia, S. Vultaggio, G. Dondio, S. Gagliardi, S. Minucci, C. Mercurio, Synthesis and biological characterization of spiro[2H-(1,3)-benzoxazine-2,4'-piperidine] based histone deacetylase inhibitors, Eur J Med Chem, 64 (2013) 273-284.

[43] G.M. Morris, R. Huey, W. Lindstrom, M.F. Sanner, R.K. Belew, D.S. Goodsell, A.J. Olson, AutoDock4 and AutoDockTools4: Automated docking with selective receptor flexibility, J Comput Chem, 30 (2009) 2785-2791.

[44] O. Korb, T. Stützle, T.E. Exner, PLANTS: Application of Ant Colony Optimization to Structure-Based Drug Design, in: M. Dorigo (Ed.) ANTS 2006, Springer, Berlin, 2006, pp. 247-258.

[45] J.J.P. Stewart, MOPAC 2012, in: Stewart Computational Chemistry, USA, Colorado Springs, CO, 2014.

[46] E.F. Pettersen, T.D. Goddard, C.C. Huang, G.S. Couch, D.M. Greenblatt, E.C. Meng, T.E. Ferrin, UCSF Chimera--a visualization system for exploratory research and analysis, J Comput Chem, 25 (2004) 1605-1612.

[47] K. Chen, L. Xu, O. Wiest, Computational exploration of zinc binding groups for HDAC inhibition, J Org Chem, 78 (2013) 5051-5055.

[48] J.J. Stewart, Optimization of parameters for semiempirical methods VI: more modifications to the NDDO approximations and re-optimization of parameters, J Mol Model, 19 (2013) 1-32.

[49] A. Klamt, G. Schüürmann, COSMO: a new approach to dielectric screening in solvents with explicit expressions for the screening energy and its gradient J Chem Soc, Perkin Trans 2, (1993) 799-805.

[50] J. Pottel, E. Therrien, J.L. Gleason, N. Moitessier, Docking ligands into flexible and solvated macromolecules. 6. Development and application to the docking of HDACs and other zinc metalloenzymes inhibitors, J Chem Inf Model, 54 (2014) 254-265.

[51] J. Baker, An algorithm for the location of transition states, J Comput Chem, 7 (2004) 385-395.

[52] The PyMOL Molecular Graphics System, Version 1.7.4 Schrödinger, LLC., in.

[53] D. Seeliger, B.L. de Groot, Ligand docking and binding site analysis with PyMOL and Autodock/Vina, J Comput Aided Mol Des, 24 (2010) 417-422.

[54] E.A. Dierks, K.R. Stams, H.K. Lim, G. Cornelius, H. Zhang, S.E. Ball, A method for the simultaneous evaluation of the activities of seven major human drug-metabolizing cytochrome

P450s using an in vitro cocktail of probe substrates and fast gradient liquid chromatography tandem mass spectrometry, Drug Metab Dispos, 29 (2001) 23-29.

[55] C.L. Crespi, V.P. Miller, D.M. Stresser, Design and application of fluorometric assays for human cytochrome P450 inhibition, Methods Enzymol, 357 (2002) 276-284.

Table 1. HDAC Enzyme and Antiproliferative Activity Data for Vorinostat and Spirochromanes **1a–c**, **15–18** and **31a–h to 34a–h**[a]

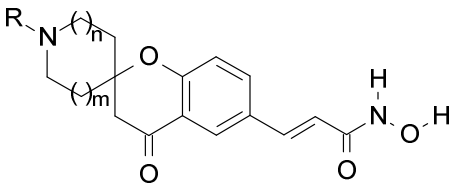

	R	m	n	Enzyme (μM)	K562 (μM)	A549 (μM)	HCT116 (μM)
	vorinostat	(see Fig 1)		0.102	0.645	1.079	0.757
1a[30]	benzyl	1	1	0.121	0.399	0.773	0.477
1b[33]	4-F-benzyl	1	1	0.108	0.681	1.32	0.777
1c[33]	Ph-$(CH_2)_2$-	1	1	0.113	0.180	0.551	0.201
15	H	0	0	0.228	2.58	8.58	3.68
31a	CH_3	0	0	0.168	0.168	0.429	0.178
31b	acetyl	0	0	0.485	15.1	47.7	10.5
31c	ethyloxycarbonyl	0	0	0.286	1.88	4.87	1.23
31d	benzyl	0	0	0.067	0.175	0.245	0.076
31e	4-F-benzyl	0	0	0.130	0.301	0.684	0.190
31f	1-methyl-*1H*-indol-3-ylmethyl	0	0	0.062	0.046	0.242	0.078
31g	Ph-$(CH_2)_2$-	0	0	0.219	0.250	0.896	0.220
31h	benzoyl	0	0	0.081	0.376	1.33	0.294
16	H	1	0	0.131	4.14	2.32	2.27
32a	CH_3	1	0	0.119	0.198	0.357	0.146
32b	acetyl	1	0	0.955	>50	>50	>50

32c	ethyloxycarbonyl	1	0	0.150	0.721	0.837	0.351
32d	benzyl	1	0	0.052	0.271	0.389	0.072
32i	(-)-benzyl	1	0	0.026	0.119	0.332	0.066
32j	(+)-benzyl	1	0	0.037	0.130	0.303	0.071
32e	4-F-benzyl	1	0	0.196	0.283	0.642	0.178
32f	1-methyl-*1H*-indol-3-ylmethyl	1	0	0.085	0.051	0.180	0.047
32g	Ph-$(CH_2)_2$-	1	0	0.027	0.102	0.272	0.043
32h	benzoyl	1	0	0.187	0.533	2.11	0.510
17	H	2	0	0.136	0.555	0.714	0.228
33a	CH_3	2	0	0.237	0.056	0.103	0.063
33b	acetyl	2	0	0.207	5.6	14.5	3.24
33c	ethyloxycarbonyl	2	0	0.232	0.936	2.28	0.678
33d	benzyl	2	0	0.056	0.430	0.839	0.385
33i	(-)-benzyl	2	0	0.084	0.441	1.063	0.326
33j	(+)-benzyl	2	0	0.143	0.523	1.461	0.447
33e	4-F-benzyl	2	0	0.034	0.552	1.16	0.372
33f	1-methyl-*1H*-indol-3-ylmethyl	2	0	0.183	0.147	0.425	0.078
33g	Ph-$(CH_2)_2$-	2	0	0.001	0.106	0.157	0.052
33h	benzoyl	2	0	0.165	2.01	4.13	1.326
18	H	2	1	0.134	5.99	3.12	1.08
34a	CH_3	2	1	0.114	0.329	0.534	0.098
34b	acetyl	2	1	0.323	5.18	20.1	3.51
34c	ethyloxycarbonyl	2	1	0.300	1.66	5.75	1.01

34d	benzyl	2	1	0.073	0.162	0.371	0.047
34e	4-F-benzyl	2	1	0.149	0.144	0.333	0.063
34f	1-methyl-*1H*-indol-3-ylmethyl	2	1	0.114	0.046	0.260	0.060
34g	Ph-$(CH_2)_2$-	2	1	0.056	0.188	0.184	0.062
34h	benzoyl	2	1	0.110	1.11	3.78	0.617

[a] Assays done in replicates ($n \geq 2$). Mean values are shown and the standard deviations are <30% of the mean

Table 2. HDAC Selectivity Profile for Vorinostat, **1a-c**, **32d** and **34d**[a]

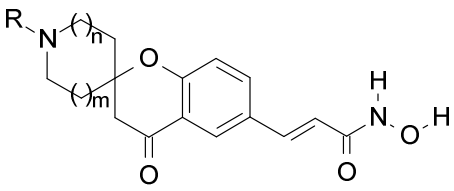

	R	m	n	Enzyme (μM)	HDAC2 (μM)	HDAC3 (μM)	HDAC6 (μM)
vorinostat		(see Fig 1)		0.102	0.197	0.055	0.029
1a[30]	benzyl	1	1	0.121	0.270	0.065	0.103
1b[33]	4-F-benzyl	1	1	0.108	0.320	0.092	0.192
1c[33]	Ph-$(CH_2)_2$-	1	1	0.113	0.199	0.130	0.138
32d	benzyl	1	0	0.052	0.082	0.028	0.123
34d	benzyl	2	1	0.073	0.072	0.030	0.151

[a] Assays done in replicates ($n \geq 2$). Mean values are shown and the standard deviations are <30% of the mean

Table 3. Microsomal Stability Data for Selected Spirochromanes[a]

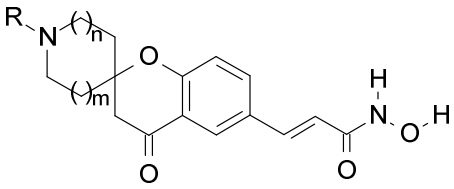

Cpd.	R	m	n	Microsomal Stability [%]		Cytochrome P450 [% inhibition at 10 μM]			
				Mouse	Human	1A2	2C19	2D6	3A4
vorinostat	(see Fig 1)			82	93	25	69	25	35
1a[30]	benzyl	1	1	32	55	5	41	56	48
1b[33]	4-F-benzyl	1	1	47	63	5	61	43	34
1c[33]	Ph-$(CH_2)_2$-	1	1	57	66	13	42	41	40
31d	benzyl	0	0	44	44	5	40	64	53
31f	1-methyl-*1H*-indol-3-ylmethyl	0	0	27	51	8	68	74	84
32d	benzyl	1	0	27	24	5	39	70	69
32i	(–)-benzyl	1	0	19	23	nd[b]	nd[b]	nd[b]	nd[b]
32j	(+)-benzyl	1	0	19	11	nd[b]	nd[b]	nd[b]	nd[b]
32f	1-methyl-*1H*-indol-3-ylmethyl	1	0	8	16	nd[b]	nd[b]	nd[b]	nd[b]
32g	Ph-$(CH_2)_2$-	1	0	31	31	5	59	41	64
33a	Me	2	0	72	42	5	12	14	51
33f	1-methyl-*1H*-indol-3-ylmethyl	2	0	23	19	nd[b]	nd[b]	nd[b]	nd[b]
33g	Ph-$(CH_2)_2$-	2	0	19	16	nd[b]	nd[b]	nd[b]	nd[b]
34a	Me	2	1	62	79	5	9	5	12
34d	benzyl	2	1	25	19	nd[b]	nd[b]	nd[b]	nd[b]
34e	4-F-benzyl	2	1	25	11	nd[b]	nd[b]	nd[b]	nd[b]

34f	1-methyl-*1H*-indol-3-ylmethyl	2	1	19	38	nd[b]	nd[b]	nd[b]	nd[b]
34g	Ph-$(CH_2)_2$-	2	1	39	27	5	81	52	41

[a] Assays done in replicates ($n \geq 2$). Mean values are shown and the standard deviations are <30% of the mean; [b] nd: not determined

Figure 1. FDA approved HDAC inhibitors.

Figure 2. Nuclear HeLa extract (Biomol N. E.) and total Hela extract were prepared and analyzed by SDS–PAGE. Level of histone decaetylases 1, 2, 3, 4 and 6 were detected using rabbit polyclonal and mouse monoclonal antibodies, followed by ECL detection.

Figure 3. Interaction between the hydroxamate-chromane moiety (the common part) and the HDAC1 structure. The secondary structure of the enzyme is depicted as well as the ligand and the neighbor residues (labeled for type and numbering) as sticks. The image is color-coded for atom-type and carbon atoms are in grey for the target and in green for the ligand. The metal coordination is also present as the main polar interaction of the complex (yellow dashed lines).

Figure 4. Hydrophobic interactions of spirochromanes with the outer portion of the target. The protein is depicted as surface (in light-grey) as well as the region of favorable hydrophobic interaction (in yellow). The ligand is in sticks representation and the carbon atoms are color-coded: green and light-green for the two stereoisomers of spiro(chromane-2,3'-piperidine) (**33i** and **33j** in Table 1). For comparison also the reference inhibitor, vorinostat, is depicted as ball-and-sticks.

Scheme 1. *Reagents and conditions*: (a) MeOH, *N*-BOC-cycloamine-one, pyrrolidine, 70°C, 4 h; (b) DMF, TEA, $Pd(OAc)_2$, $P(o\text{-}tol)_3$, methyl acrylate, 100°C, 3 h; (c) dioxane/H_2O, NaOH, RT, overnight or for **12** and **14** AcOH/HCl, 85°C, 3 h, then CH_2Cl_2, TEA, BOC_2O, RT, 1 h; (d) CH_2Cl_2, EDC, HOBt, TEA, NH_2OTHP, RT, overnight; (e) CH_2Cl_2, Et_2O, HCl, RT, 1 h or for **15** CH_2Cl_2, dioxan, HCl, RT, overnight.

Scheme 2. *Reagents and conditions*: (a) dioxane, HCl, RT, 1 h; (b) for **23a-26a**, **23d-26d**, **23e-26e**, **23f-26f**, **23g** and **25g** , R'CHO, $NaBH(OAc)_3$, RT, 2 h; for **23b-26b**, **23c-26c**, **23h-26h** , RCl, DIPEA or TEA, RT, 1 h; for **24g** and **26g** , Ph-$(CH_2)_2$-Br, DIPEA, RT, 8 days for **24g** and 15 days for **26g**; (c) AcOH/HCl, 85°C, 3 h or for **27b**, **27c**, **27f**, **27h**, **29b**, **29e-h**, and **30e-f**, dioxane/H_2O, NaOH, RT, overnight; (d) , EDC, HOBt, TEA, NH_2OTHP, RT, overnight; (e) , Et_2O, HCl, RT, 1 h or for **31b-c**, **31e-g**, **33b**, **33f-g** and **34f** , dioxan, HCl, RT, overnight.

Scheme 3. *Reagents and conditions*: (a) , EDC, HOBt, TEA, (S)-2-(6-methoxynaphthalen-2-yl)propionic acid, RT, overnight; (b) AcOH, 6 N HCl, MW, 120°C, 3 h; (c) CH_3OH, H_2SO_4, reflux, overnight; (d) C_6H_5CHO, $NaBH(OAc)_3$, RT, 2 h; (e) CH_3COOH, 6 N HCl, 85°C, 3 h; (f) CH_2Cl_2, EDC, HOBt, TEA, NH_2OTHP, RT, overnight; (g) CH_2Cl_2, Et_2O, HCl, RT, 1 h.

Scheme 4. *Reagents and conditions*: (a) CH_2Cl_2, dioxane, 4 M HCl, RT, 5 h; (b) CH_2Cl_2, EDC, HOBt, TEA, (R)-2-acetoxy-2-phenylacetic acid, RT, 18 h; (c) C_2H_5OH, 12 N HCl, reflux, overnight; (d) CH_2Cl_2, BOC_2O, TEA, RT, overnight; (e) DMF, TEA, $Pd(OAc)_2$, $P(o\text{-}tol)_3$, methyl acrylate, 100°C, 8 h; (f) CH_2Cl_2, dioxane, HCl, RT, 3 h; (g) C_6H_5CHO, $NaBH(OAc)_3$, RT, 2 h; (h) dioxane/H_2O, NaOH, RT, overnight; (i) CH_2Cl_2, EDC, HOBt, TEA, NH_2OTHP, RT, overnight; (j) CH_2Cl_2, Et_2O, HCl, RT, 1 h.

Figure 1.

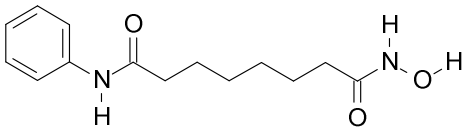

vorinostat

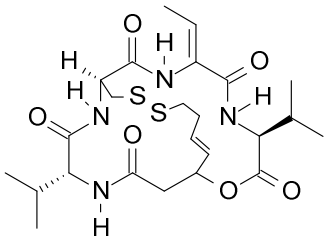

romidepsin

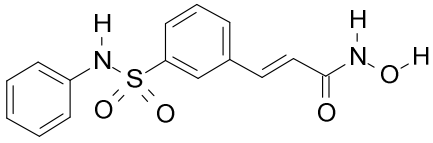

belinostat

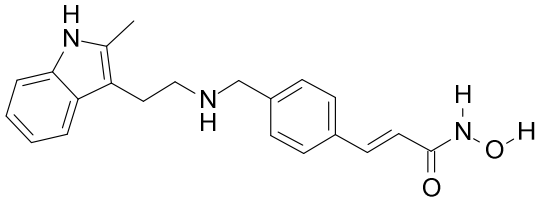

panobinostat

Figure 2.

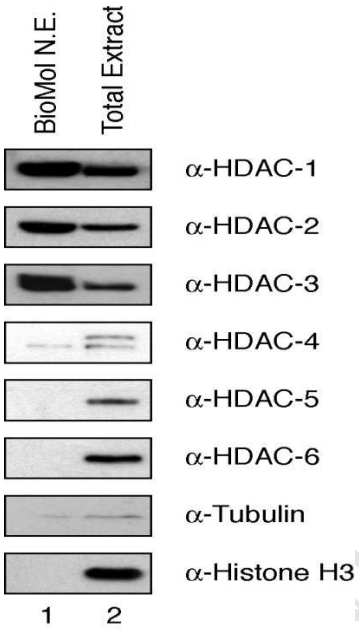

Figure 3.

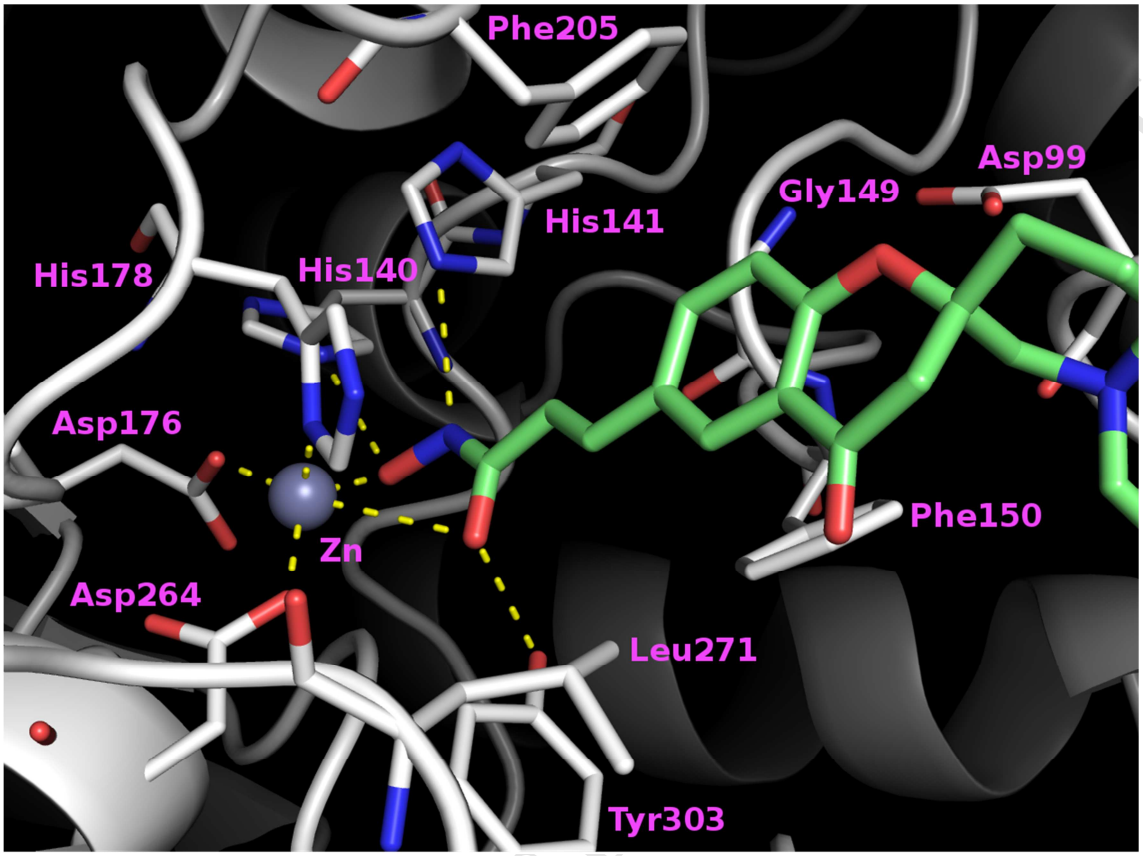

Figure 4.

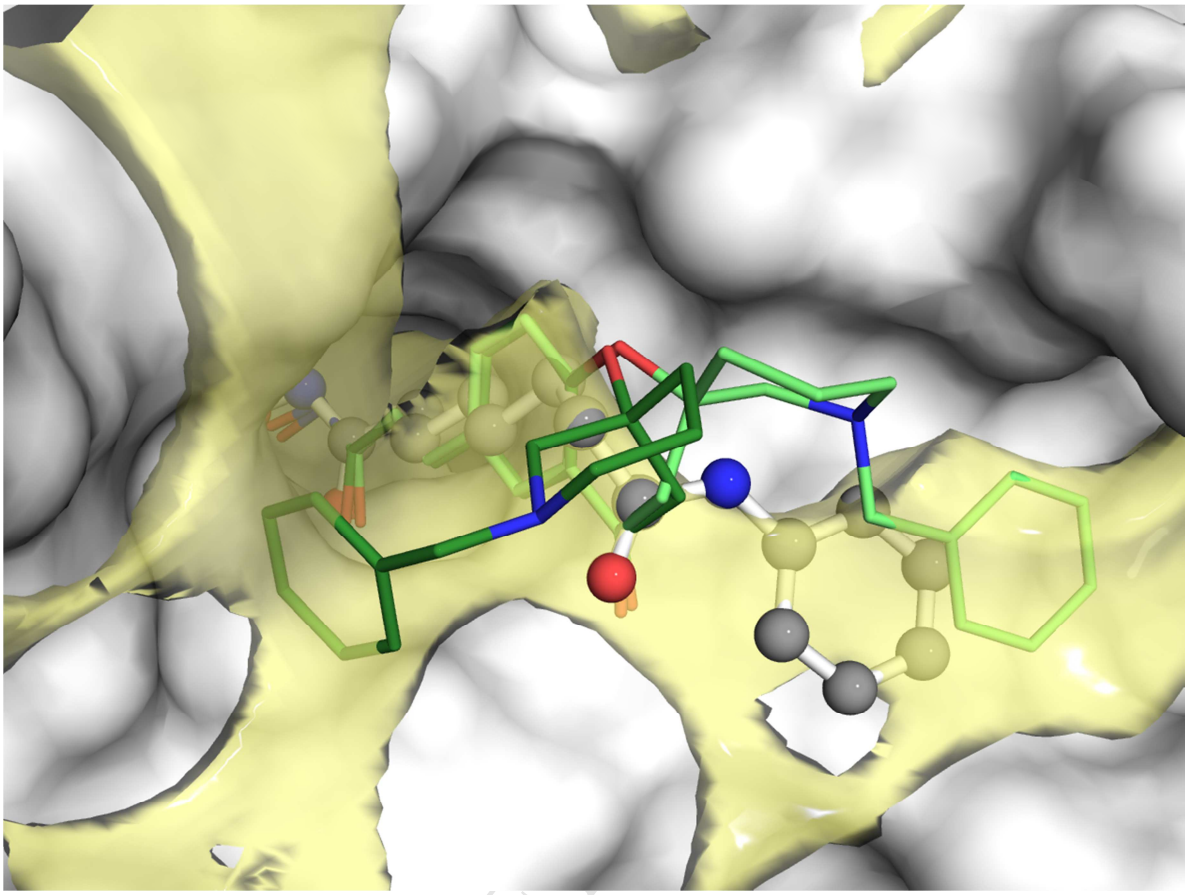

Scheme 1.

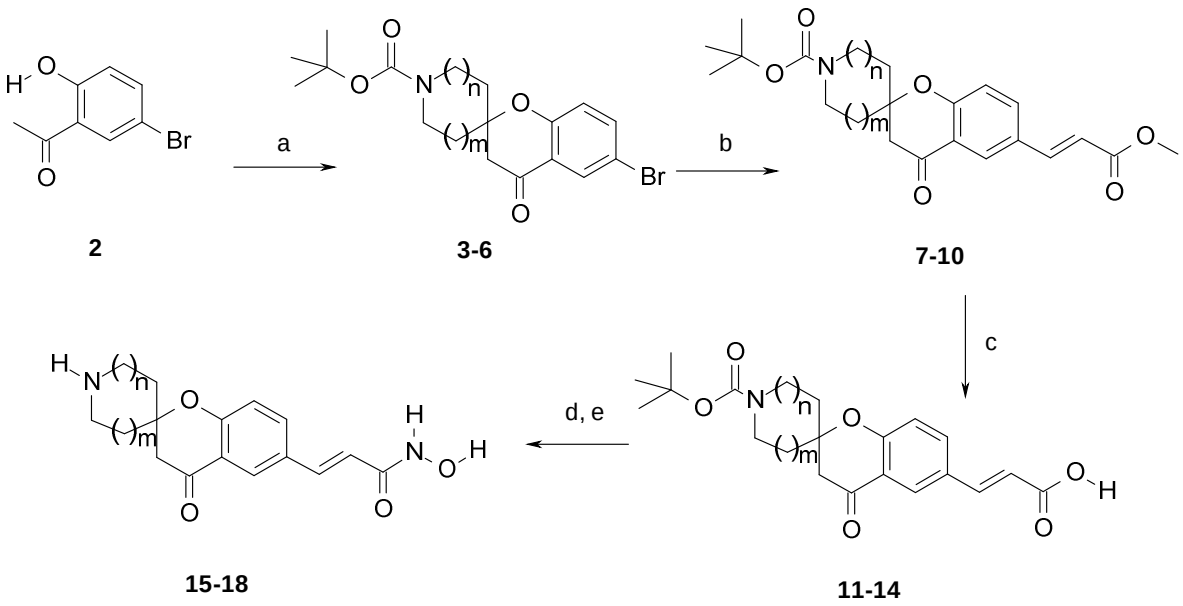

Scheme 2.

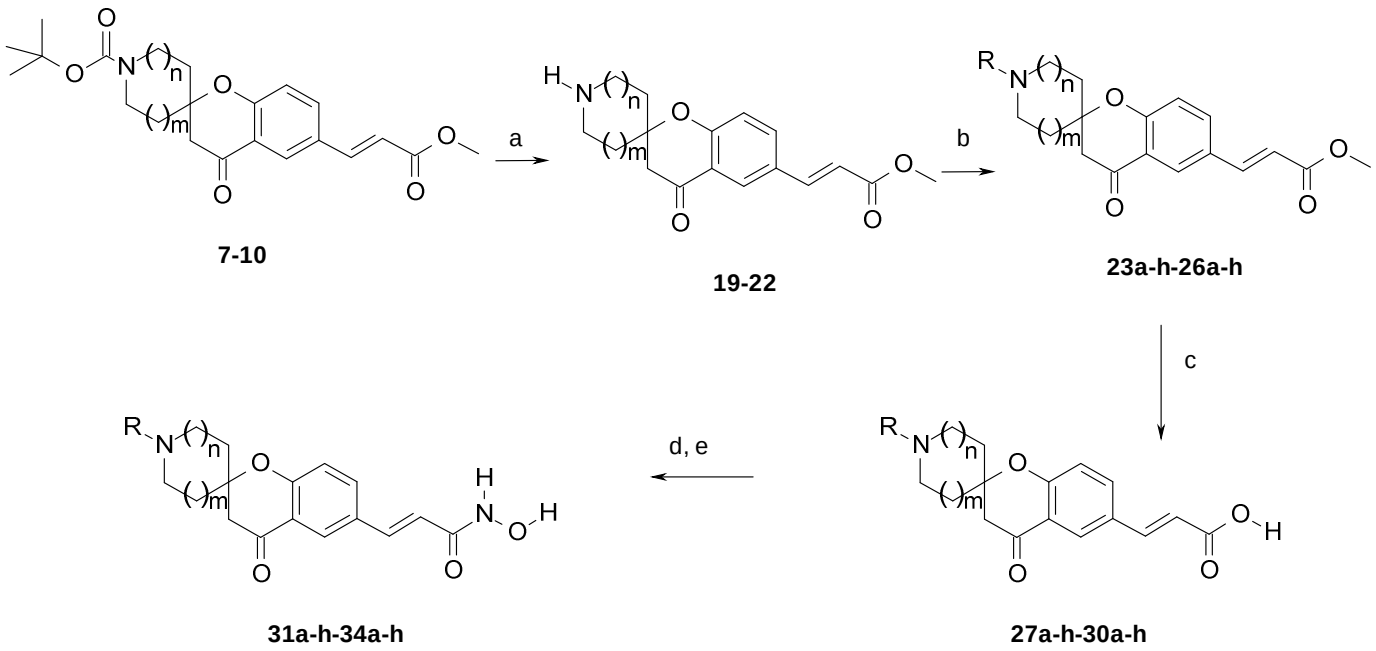

Scheme 3.

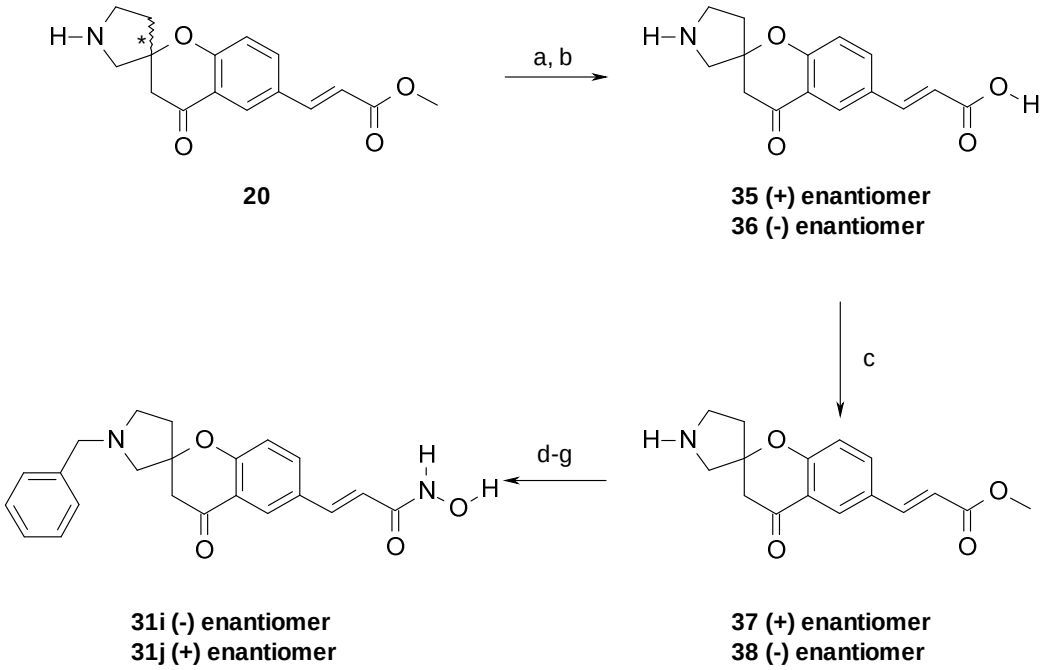

20

35 (+) enantiomer
36 (-) enantiomer

37 (+) enantiomer
38 (-) enantiomer

31i (-) enantiomer
31j (+) enantiomer

Scheme 4.

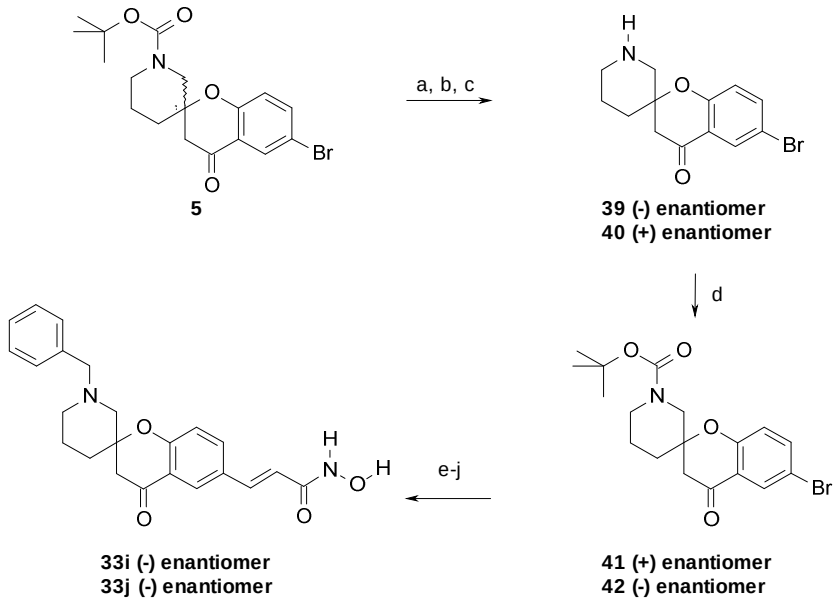

5

39 (-) enantiomer
40 (+) enantiomer

41 (+) enantiomer
42 (-) enantiomer

33i (-) enantiomer
33j (-) enantiomer

Research Highlight

- A spirochromane hydroxamate scaffold was designed and evaluated for its HDAC inhibition.
- Several inhibitors displayed potent antiproliferative activity in tumor cell lines.
- Molecular modeling studies were carried out to unravel the binding mode of these inhibitors.
- Selected compounds showed good microsomal stability.